UNIVERSITY OF CALIFORNIA
RIVERSIDE

The Role of the Surface Roughness and Filler Size on Performance of Graphene-Based Thermal Interface Materials

A Thesis submitted in partial satisfaction
of the requirements for the degree of

Master of Science

in

Electrical Engineering

by

Sriharsha Sudhindra

September 2021

Thesis Committee:
Dr. Alexander A. Balandin, Chairperson
Dr. Fariborz Kargar
Dr. Xi Chen

The Thesis of Sriharsha Sudhindra is approved by:

_____

_____

_____

Committee Chairperson

University of California, Riverside

Acknowledgements

Firstly, I feel privileged and would like to express my very sincere gratitude and appreciation to my advisor, Dr. Alexander A. Balandin, for giving me the opportunity to work under his supervision and providing valuable support and advice for my courses, research and future career throughout my master's study. I would also like express my sincere gratitude to Dr. Fariborz Kargar for his guidance, motivation and immense support for my research and I thank him for serving on my thesis committee. I also thank Dr. Xi Chen for being a part of the thesis committee. It has been my most cherished honor to be a part of Phonon Optimized Engineered Materials (POEM) Lab working with such smart, active, friendly and helping lab members. I would especially like to thank Zahra Barani, Dylan Wright, Dr. Jacob Lewis, Saba Baraghani and Dr. Sahar Naghibi for their support for my research. A special acknowledgement to Dr. Claudia Backed from Heidelberg University, Germany and Dr. Aleksey Drozdov from Aalborg University, Denmark for their insights and contribution to my work presented in this thesis. Some of the figures presented in this thesis is from a collaboration with them. I would also like to thank the other group members as well for supporting me in this journey. I would like to thank University of California – Riverside, Department of Electrical and Computer Engineering, for giving me the opportunity to be a part of this beautiful institute. Last but not the least, I would like to thank my parents, teachers and friends for their immense support and trust throughout these years.

Parts of this dissertation are concerned with topics presented in or reprinted from the following journal and pre-print articles:

- Sudhindra, S.; Kargar, F.; Balandin, A.A. Noncured Graphene Thermal Interface Materials for High-Power Electronics: Minimizing the Thermal Contact Resistance. *Nanomaterials* **2021**, *11*, 1699.
- Sudhindra, S.; Rashvand, F.; Wright, D.; Barani, Z.; Drozdov, A.D.; Baraghani, S.; Kargar, F.; Balandin, A.A. Thermal Transport in Graphene Composites: The Effect of Lateral Dimensions of Graphene Fillers. *Archive 2108.08409* **2021**, 1-38.

ABSTRACT OF THE THESIS

The Role of the Surface Roughness and Filler Size on Performance of Graphene Based Thermal Interface Materials

by

Sriharsha Sudhindra

Master of Science, Graduate Program in Electrical Engineering
University of California, Riverside, September 2021
Dr. Alexander A. Balandin, Chairperson

In the first part of this thesis, I present the results of my investigation of thermal characteristics of the silicone-oil based thermal interface materials (TIMs) with randomly oriented graphene and few-layer graphene fillers. The graphene TIMs were applied between surfaces with different degrees of roughness. It was found that the thermal contact resistance depends on the graphene loading, ξ, non-monotonically, achieving its minimum at the loading fraction of $\xi\sim$ 15 wt.%. Decreasing the surface roughness by ~1 μm results in approximately the factor of ×2 decrease in the thermal contact resistance for this graphene loading. The obtained dependences of the thermal conductivity, thermal contact resistance, and the total thermal resistance of the thermal interface material layer on the loading fraction and roughness can be utilized for optimization of graphene TIMs for specific materials and roughness of the connecting surfaces. In the second part of the thesis, I evaluate the performance of graphene TIMs with different filler sizes. It was established that with increase in the size of the fillers, the thermal conductivity of silicone-oil based TIMs increases. The experimentally obtained values of the thermal conductivity were fitted

with the theoretical model. It was also found that the thermal contact resistance (TCR) of the TIMs decreases with increasing filler size. The obtained results are important for development of non-cured TIMs for applications in thermal management of high-power density electronics.

Table of Contents

List of Figures

List of Tables

Chapter 1

1.1 Motivations

The miniaturization of devices has an impact on the electronics industry since mid-20th century while following the path paved out by Moore's law [1]. Expectations of earlier mobile devices were simple and limited to making a phone call for communication purposes but that is not the same in the modern advancements of smart phones and tablets alike available in the market where a device is required to perform multiple tasks including video calling, listening to music, taking pictures and gaming to name a few and also sometimes it is required to multitask. To meet such requirements, the devices make use of processors which have to be faster, cheaper, reliable and long lasting. The speed of a processor had increased 18,500 times after three decades since its introduction in the 1970's [2]. In previous iterations of microprocessors, the driving force were processor and memory for energy efficiency [3,4]. Based on the trend from the past few decades, the performance of a microprocessor was expected to increase by 30x in the year 2020 and is also projected to increase by 1000x by the year 2030 according to industry expectations [5]. So, it is evident that the microprocessor market will acquire a major portion of GDP for countries in the business for the years to come. This makes the market growth exponential.

One should realize that the size of devices has rapidly decreased and continues to do so over the years from microscale to nanoscale [6]. Modern approaches like three-

dimensional chip stacking and multi-core architectures are expected to improve the processing speed of a device without relying on the device size [7,8]. This gives the ability to make previously thought unrealistic modern devices a reality in the foreseeable future. Available reports show that the shrinking size of the overwhelming number of transistors have the capability to encounter modern computing challenges at the expense of power dissipation in a device [9–11] where the consumption can be more than expected. These modern devices generate hot spots as they operate at ultra-high frequencies where the working power is ten times higher than the advised average [12], which may result in the device not reaching its expected potential. The applications for such devices can be vast with importance in medicine, automobiles, cosmetics, textiles and personal electronics to name a few. An important factor to achieve this required goal is heat dissipation, which ensures robust performance and long life of the device. The reliability of a device or component is dependent on its operating conditions at high temperature [13]. Increasing device temperature results in an exponential increase in the rate of device failure [14]. The use of reliable thermal interface materials (TIMs) can be utilized in the electronics industry by helping the devices reach its manufactured, marketed and expected potential if not more.

The commercially available and commonly used electronic devices although do last for a very long time do not have the same response for the DoD systems as they operate at parameters exceeding that of the specified thus resulting in its early failure [15]. Using a suitable TIM becomes a top most priority in this aspect of the longevity of these systems thus also being reliable. Although DARPA's 2008 launched thermal ground plane (TGP) [16] and 2009 launched nanothermal interfaces trust (NTI) [15] which are a part of their

thermal management technologies (TMT) program have achieved commendable progress and results, the study of epoxy based 2D material TIMs with respect to its mating surface properties will help them in adapting the related finding to their present and future applications thus improving the quality of them.

1.2 Effect of Roughness on Heat Transfer

Thermal management of microprocessors in modern electronic devices like tablets and laptops alike rely on heat sinks attached on chip which is cooled by systems located remotely [17]. Hence, decreasing the temperature of the device when necessary across a junction is a priority. Heat transfer is a culmination of various concepts including, bulk thermal resistance due to the thermal conductivity of the materials in the path of heat flow and thermal contact resistance (TCR) between the actual points of contact across the two surfaces.

As well know, less than 2% of the overall area interact with each other when two surfaces are placed in contact [17,18] and the remaining is occupied by air with a thermal conductivity of 0.026 $Wm^{-1}K^{-1}$ at room temperature [19] which is not a good conductor of heat. Thus, the removal of air between the two surface becomes evident for the optimal functionality of the device and can be achieved only by utilizing a material with a higher thermal conductivity than that of air. The introduction of a reliable TIM becomes crucial in such a scenario. Also, as pointed out earlier, a good understanding of TCR will help one to tackle the problem of heat flow between two rough surfaces.

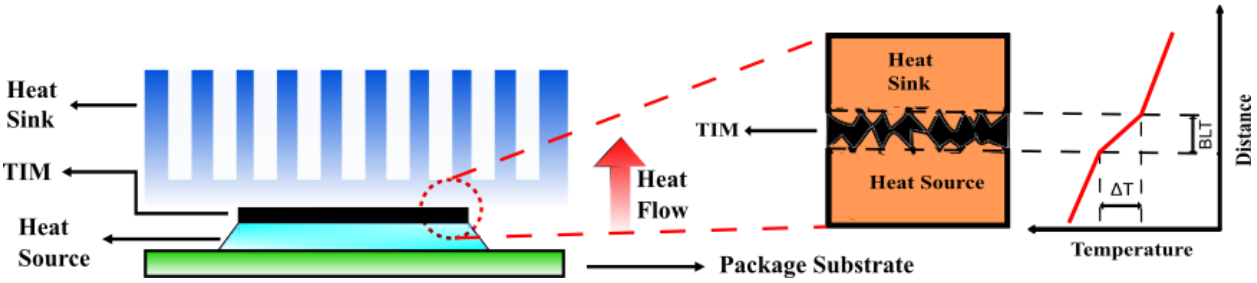

Figure 1.1: Schematic representation of TIM. Adapted from Ref. [20]: Sudhindra, S.; Kargar, F.; Balandin, A.A. Noncured Graphene Thermal Interface Materials for High-Power Electronics: Minimizing the Thermal Contact Resistance. *Nanomaterials* **2021**, *11*, 1699.

Roughness can be described as the measurement of the microscale variations in the height profile of a physical surface. This is not similar to the large-scale variations which can be a part of the surface morphology [21]. From Figure 1.1, the total thermal resistance of TIM (R_{TIM}) can be obtained [22–25]:

$$R_{TIM} = \frac{BLT}{k_{TIM}} + R_{C1} + R_{C2} \tag{1.1}$$

Here, BLT is the bond line thickness which is nothing but the thickness of the TIM, k_{TIM} is the thermal conductivity of the TIM and R_{C1} and R_{C2} are the thermal resistances of the two contact surfaces sandwiching the TIM. The values for the thermal resistance of the two surfaces can be obtained with the use of thickness and thermal conductivity of the two surfaces individually.

Hence, the total TCR of the structure can be obtained by using the following expression,

$$R_{total} = R_{C1} + R_{TIM} + R_{C2} \tag{1.2}$$

TCR is known to be a factor of surface roughness, interface pressure, applied temperature and viscosity [24]. TCR at the interface of two surfaces play a major role in heat transfer in multiple engineering applications [20,26–29]. Thermal contact conductance (TCC) can also be determined as it is the reciprocal of TCR. Many simulations and models have been presented in earlier studies along with multiple experimental studies as well [30–33] and they present their results by telling that heat loss increases with increase in surface roughness between the two surfaces. An increase in the surface roughness increases TCR [34] and decrease in TCC [35,36] A study was conducted by another group which included both experimental and theoretical analysis to understand the concept of total thermal resistance and it was concluded that the results were reasonably similar with an error of less than 6.5% [37].

Researchers have used metal meshes for improving the roughness of a surface to deal with the problem of heat transfer [38] but this technique cannot be used in all applications and hence understanding the influence of surface roughness on heat transfer is crucial. The process of temperature drop across an interface in bulk materials is dependent surface roughness as well as an atomically smooth surface is not inherent for the interface thus the impact of a temperature variation may play a major role in understanding the basic concepts of heat transfer.

The use of a TIM is ideal for such rough surface as improving the quality of the surface roughness can turn out to be cost effective. A previous work has shown that the roughness of the TIM along with the roughness of the surface also affect the TCR [39]. A method to reduce the interfacial thermal resistance between graphene and copper substrate

by 17% with the help of engraving the copper surface with nano-pillared patters has also been show which is contrary to the conventional method of understanding the surface roughness [40] When a suitable TIM is not used, the interface consists of air and this is the interface material and the temperature difference across the interface increases but this is not the case a TIM is used where the temperature difference is reduced by 52-55 times than that of air between the two rough surfaces [41].

Computational fluid dynamics (CFD) is a commonly used analysis software to study the thermal design in electronics where the electrical resistance can be determined faster than the TCR and the electrical resistance can be used to determine the TCR is a shorter period of time [42]. For surfaces with higher roughness, the electrical resistance was found to be constant [42]. Researchers have also used the Wiedemann-Franz law to study and relation between electrical resistance and thermal resistance and it was found that the two resistances decrease with increase in pressure where the electrical resistance was dependent on the methods of surface processing and the thermal resistance is dependent on the air gap between the two surfaces [43].

1.3 Effect of Filler Size on Heat Transfer

Understanding the performance of heat transfer as a function of the filler size in composites is an important aspect of study but to the contrary, there are limited previously reported studies addressing this subject [44–46]. It was also established in other studies that the size of the fillers plays an important role in the percolation threshold of composites [47–49]. An important practical aspect that has to be remembered is the maximum lateral dimension

of fillers in a composite where a large size would affect the thermal performance due to bending of the fillers and thus leading to an increase in BLT. There have also been studies which deal with other factors of the size of fillers which affect the performance which include defect density [50–53], specific surface area and interface area between the polymer matrix and the filler [54–58], and the kapitza resistance [59]. Thus, it becomes important to utilize extremely well-prepared fillers in composites to experimentally understand the effect of filler size on the heat transfer performance of composites.

1.4 Thermal Interface Materials

A common technique to decrease the value of the overall TCR is by using a TIM layer with high thermal conductivity [29,60–62]. Although the thermal conductivity of the material is an important factor for determining its performance, it should be evaluated being sandwiched between desired surfaces to understand its true performance [63–66]. Commercially available TIMs do not meet the growing industry requirements [67] and have to updated to suit the same. A common technique in order to achieve this is polymer filler based TIMs in which the loading faction of the material along with the overall thickness of the TIM can be controlled to meet the necessary goal. The thermal resistance of the TIM also increases with its thickness regardless of other parameters mentioned in the previous sections [68]. The polymer filler based TIMs can be prepared in the cured or the non-cured based on required application where the thermal percolation of the two differ from each other [69]. An emerging application for the non-curing TIMs is in the field of

solar cells [70–72]. A few other types of TIMs available are solder, grease, thermal pads, phase change materials and carbon based.

1.5 Graphene as Fillers for TIMs

First mechanically exfoliated from graphite in 2004 [73], graphene is a one atom thick allotrope of carbon with extraordinary properties in electrical and mechanical applications [73–77] along with thermal properties exhibiting high intrinsic thermal conductivity of 2000 ~ 5300 W/mK near RT based on flake quality and dimensions [50,78–84]. It has been both theoretically and experimentally shown that graphene has a high electron mobility [85,86]. The thermal conductivity of graphene is based on phonons and varies with temperature where the majority of the contribution for the overall thermal conductivity is from longitudinal acoustic phonons [87]. There is an overgrowing demand for better heat dissipation for the modern advancements in the electronics industry [29,61,62,88–91]. This demand can be met by updating the quality of a TIM. One of the upcoming methods for achieving the needful task is a polymer-graphene filler-based TIM. Although polymers have a low thermal conductivity of 0.2 – 0.5 W/mK [92], incorporating them with graphene would enhance its overall thermal conductivity as they are compatible with each other's matrix allowing the value to exceed 12.5 W/mK which is higher than that of commercially available TIMs [67,93] where an interesting aspect of a graphene filler-based TIM is the improvement of thermal conductivity of the matrix over the period of thermal cycling [89]. It has also experimentally been shown that graphene can be used for hybrid composites with boron nitride [94] and with copper nanoparticles [95] which results

in obtaining a thermal conductivity value higher than that of commercially available TIMs. The use of graphene-FLG fillers have an advantage over graphite fillers as they conform well with the matrix and also have an interesting feature of flexibility over the thick graphite-based fillers [61]. Graphene is preferred as fillers over CNTs as well in thermal composites for its extremely wonderful coupling with matrix materials and affordable cost [90]. This has led to the use of such composites in various applications over the past few years [23,24,29,63,67,69,71,72,83,89,91,93–102].

Chapter 2

2.1 Experimental Setup

This chapter describes the instruments used along with recipe used to prepare silicone-oil based graphene and few-layer graphene filler non-cured TIMs. Sections of this chapter have been separated accordingly to explain both projects explained in this thesis. For the first research on the influence of surface, Filmetrics ProFilm 3D Optical Profilometer was used to study the copper plate surface roughness while a Allied High-Tech Products polisher was used to induce roughness to these plates. In order to study the thermal properties of the prepared composites, LongWin LW-9389 TIM Tester was utilized.

For the second research explaining the influence of filler size on the thermal performance of the composites, liquid phase exfoliation was performed to acquire fillers of different sizes. Theses characteristic properties of the acquired fillers were extracted from an atomic force microscope and verified by Raman spectroscopy. The prepared composites with these fillers were also tested using the LongWin LW-9389 TIM Tester. A detailed description of each equipment item and its working principles are given below.

2.1.1 Optical Profilometer

The Filmetrics ProFilm 3D Optical Profilometer can be used to obtain topographical information of a specimen within seconds. It makes use of both white light interferometry (WLI) and phase-shifting interferometry (PSI) techniques with an objective lens to study

the specimen and provides two-dimensional, three-dimensional and quantitative information without contacting the surface. As the equipment makes use of a non-contact technique, it can measure even curved samples which is difficult of stylus-based techniques. The quantitative data acquired can be reliable with the step height measurements can be measured in the range of 0.1 nm to 10 mm and a blue LED to scan the surface. The equipment makes use of interference fringes to determine the geometry of the surface. For this study, a 50× Nikon lens was utilized. The commonly used surface roughness parameter in this equipment is the root mean square roughness (S_q) and the numerical value is determined using the formula [103]:

$$S_q = \sqrt{\frac{1}{A}\iint^{A} Z^2(x,y)\,dx\,dy} \tag{2.1}$$

Where, *A* is the area and *Z(x,y)* is the surface profile amplitude.

2.1.2 Thermal Characterization

LongWin LW-9389 TIM tester (LongWin Science and Technology Corp, Taiwan) is based on ASTM D 5470-06 standard which is capable of measuring thermal resistance, thermal impedance and apparent thermal conductivity of both homogeneous and heterogeneous samples using the Fourier's law with a very less error margin. The sample is placed between two temperature differential plates which enables the procedure of heat transfer. The thermal properties of the base polymers can be determined with varying thickness as well. The instrument can be used to determine the thermal properties for varying pressure and temperature making it a reliable instrument to study the long-term durability of a TIM.

The ASTM D 5470-06 can be used to classify the pressure while utilizing the hardness of the material used. It is noted that the pressure difference between soft and hard [104]. One should also note that the ASTM D 5470 standard in general can be used to measure thermal conductivity of the specimen in the range of 0.1-10 W/mK [105] while having the capability of measuring its thermal contact resistance as well.

2.2 Investigated Material Systems

2.2.1 Copper Plates

A commonly used copper substrate has proved to have broad applications in the electronics industry [97,106,107]. For the experiments, 1-inch X 1-inch copper plates were used with a uniform thickness of 1.09 mm (Midwest Steel Supply, USA). To induce roughness to these copper plates, a Metprep 3 polisher (Allied High-Tech Products, Inc, USA) were used with an 8-inch, 180 grit silicon carbide paper discs.

2.2.2 Graphene Fillers

The xGnP® Graphene (H25) fillers used for the measurements were acquired from XG-Sciences Inc (Lansing, MI, USA) which have an average thickness of up to 15 nm with lateral dimension of 25 μm. The graphene powder is 99% pure, with density of 2.2 g/cm^3 and a typical surface area of 50 m^2/g to 80 m^2/g [108].

2.2.3 Graphene Fillers

For this project, the graphene fillers were prepared by the technique of probe sonication of the commercially acquired graphite powder (Sigma Aldrich 496596) with an initial concentration 40 gL^{-1} in an aqueous sodium cholate (SC) solution. The graphite powder was introduced to a 80 mL aqueous surfactant solution (C_{surf}= 6 gL^{-1}) in a stainless-steel beaker. The prepared mixture was subjected to sonication in a two-step procedure which serves the purpose of removing impurities which might be present in the powder. The first step included the prepared mixture being sonicated for 1 hour at a 60 % Amplitude with a 8s on and a 2s off pulse sequence with a Sonics Vibracell VCX 500 (500 W) and a threaded probe and a replaceable tip. The graphene dispersions were kept in a 5 °C cryostat cooled water bath to avoid heating of the sample during the process of sonication. After the procedure, the graphene dispersion was centrifuged with 3800 *g* for 1.5 h in a Hettich Mikro 220R centrifuge which is equipped with a 1016 fixed-angle rotor at a temperature of 15 °C. The supernatant containing the water-soluble impurities were discarded and the sediment was redispersed in a 80 ml of 2 gL^{-1} aqueous surfactant solution. In the second step, the graphene dispersion again sonicated for a duration of 5 h at 60 % Amplitude with a 6s on and 2s off pulse sequence.

For the selection of the filler size, the technique of liquid cascade centrifugation with sequentially increasing rotation speeds of 2 hrs each step at a temperature of 15°C was used. After each centrifugation step, the supernatant and the sediment were separated and the sediment was collected in a reduced volume (~10 mL) and surfactant concentration (0.1 gL^{-1}) and the supernatant was subjected to a centrifugation at higher speeds. The

centrifugation conditions are expressed as relative centrifugal field (RCF) in units of the earth's gravitational force, *g*. The process of centrifugation was performed with the help of a JA25.50 fixed angle rotor with a Beckman Coulter Avanti centrifuge at 15°C for 2 hrs with 50 mL centrifuge tubes (VWR, order number 525-0402) filled with 20 mL of graphene dispersion each. The RCF used were 30, 200 and 2500 *g* and the supernatant after 2500 g was discarded. The sediments after the centrifugation step at 30 g contained the largest sheets but also unexfoliated bulk material. In order to separate the two, the dispersions were allowed to settle for 16 hrs and the top 80% of the volume were decanted and collected. This sample was denoted as "large" graphene fillers. "Medium" fillers refer to the sample being trapped between 30 and 200 *g* centrifugation, while the "small" fillers denotes the sample that were obtained from centrifugation process between 200 and 2500 *g*. The exfoliation and size selection procedures were repeated 4 times over in order to produce a sufficiently large mass of fillers. The same fractions of all the batches were combined.

In the final step, the filler was transferred to t-Butoxymethyl-oxiran as a solvent for better compatibility with the process of composite preparation. The combined fractions of fillers were centrifuged at 3000 *g* for 2 hrs and the clear supernatant was removed and the sediment was redispersed in the solvent.

2.2.4 Polymer Matrix

For both the research projects, silicone oil (Fisher Scientific, USA) was chosen as base polymer, also commonly regarded as PDMS – Poly(dimethylsiloxane).

2.3 Experimental Procedures

2.3.1 Preparation of TIMs

The non-cured TIMs with graphene fillers studied for this research project were prepared from commercially available FLG flakes with specifications mentioned in section 2.2.2 and with the base polymer of silicone oil mentioned in section 2.2.4. The mixture of graphene and FLG and silicone oil were weighed in a small cylindrical container to obtain the desired filler concentration in each TIM sample intended in this study. In order to maintain the quality and size of the fillers, acetone was added. This ensures that the fillers would not agglomerate during the process of mixing [109]. The solution was mixed at a speed of 300 rpm for 20 min using a high-speed shear mixer to obtain a homogenous distribution of the fillers in the polymer matrix. In order to evaporate the added acetone, the prepared compound was introduced to an oven at a temperature of ~70 ºC for a duration of 2 hrs. It is important to note here that the role of acetone is only to assist in the homogenous dispersion of fillers in the prepared compound and thus should no be used in testing of each TIM [20,69].

2.3.2 Preparation of TIMs

The exfoliated graphene fillers as explained in section 2.2.3 were centrifuged in its solvent with a speed of 7000 rpm for a duration of 2 minutes. This ensured that the fillers were allowed to be separated from its solvent and this was confirmed by visual inspection. The

solvent was removed from the vial into a petri dish with the help of a dropper to the best of my ability. The remaining solution was transferred under a fume hood into another petri dish and was allowed to evaporate for 24 hours at room temperature. This process ensured the removal of the solvent thus leaving us with only the graphene fillers. These obtained fillers were measured and mixed with the base polymer of silicone oil to prepare the studied non-cured TIMs with a high-shear speed mixer at a speed of 2000 rpm for 10 minutes and then with a speed of 3000 rpm for a duration of 15 minutes. This ensured a homogenous distribution of the fillers in the base polymer. This process was repeated for all the studied TIMs in this research project.

2.3.3 Testing of the Synthesized TIMs

The prepared TIMs in both the projects were tested using the mentioned TIM tester in section 2.1.2. The non-cured TIMs were tested under a pressure of 80 psi and a temperature of 80 ºC for a duration of 40 minutes for each thickness (BLT). To achieve different BLTs, red plastic shims (Precision Brand Products Inc, USA) were used. A schematic of the TIM tester is presented in Figure 2.1.

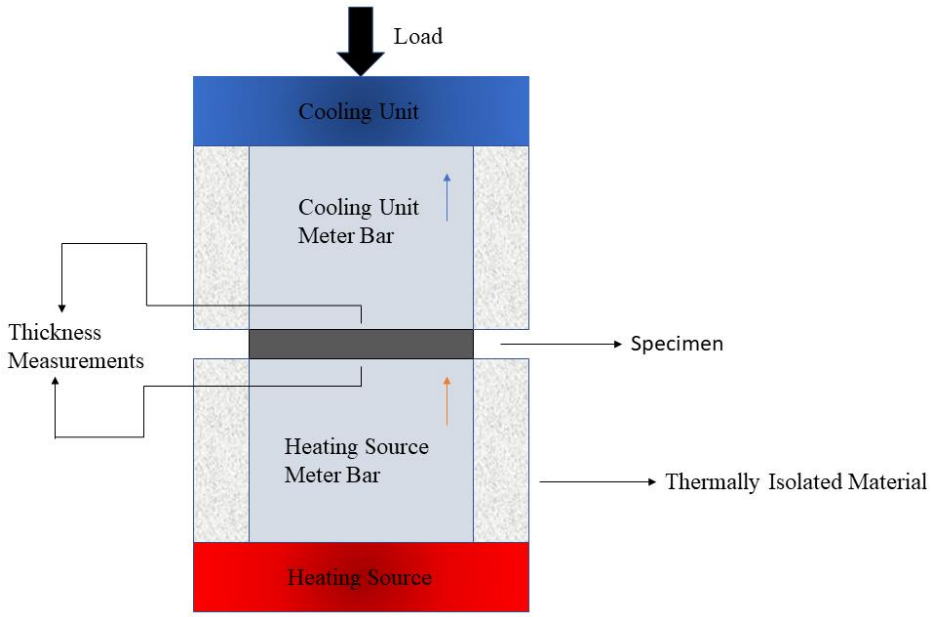

Figure 2.1: Schematic representation of LongWin TIM Tester. Adapted from supplementary information of Ref. [20]: Sudhindra, S.; Kargar, F.; Balandin, A.A. Noncured Graphene Thermal Interface Materials for High-Power Electronics: Minimizing the Thermal Contact Resistance. *Nanomaterials* **2021**, *11*, 1699.

The specimen (TIMs in our case) in interest is placed between the hot and cold meter bars and when the heat flow is initiated. The heat flux will travel from the hot meter bar towards the cold meter bar while passing the specimen in between. The Fourier's law can be used with the data acquired to calculate the necessary key aspects of the specimen. The thermal imperdance is calculated by the TIM tester's software which allowed us to determine the thermal properties of the synthesized TIMs.

Chapter 3

3.1 Results and Discussions

3.1.1 Analysis of the Surface Roughness

Figure 3.1 presents the results of the roughness of the copper plates measured using the profilometer. The copper plate in Figure 3.1(a) was not polished by the polisher described in section 2.2.1 and was used as a reference. To induce roughness to the copper plates presented in Figure 3.1 (b), (c) and (d), the plates were polished at a speed of 100 RPM for ~1 minute, ~2.5 minutes and ~3.5 minutes respectively. The areal root mean square (RMS) roughness, S_q, determined for these plates were 0.05 µm, 1.2 µm, 2.5 µm and 3.1 µm, respectively. The preparation of the surfaces and the profilometer measurements enabled the investigation of the effect of roughness on the thermal contact resistance with graphene TIMs.

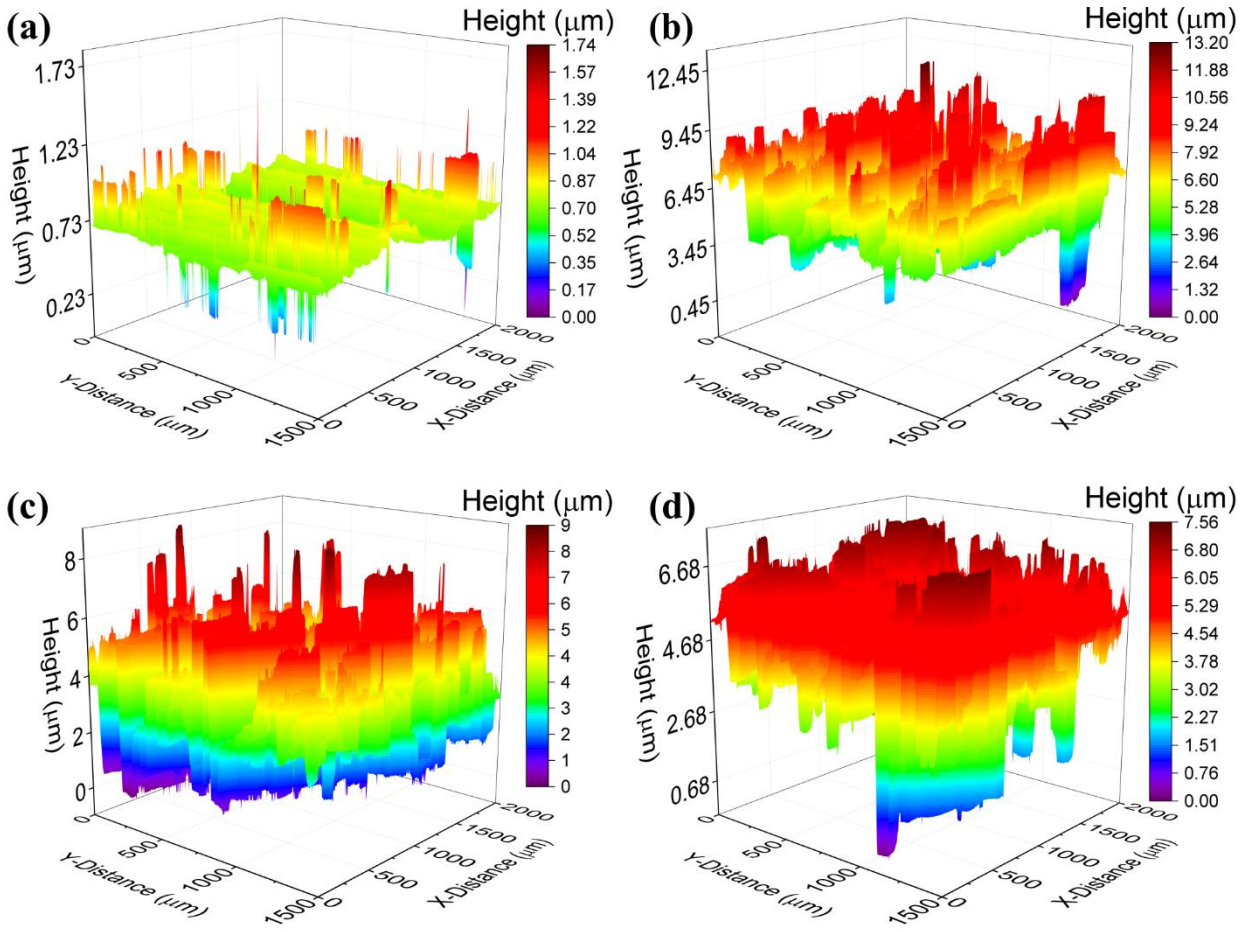

Figure 3.1: Roughness characteristics of the copper plates determined by an optical profilometer. The plates have the following root mean square (RMS) roughness: (a) S_q=0.05 μm, (b) S_q=1.2 μm, (c) S_q=2.5 μm, and (d) S_q=3.1 μm. Adapted from Ref. [20]: Sudhindra, S.; Kargar, F.; Balandin, A.A. Noncured Graphene Thermal Interface Materials for High-Power Electronics: Minimizing the Thermal Contact Resistance. *Nanomaterials* **2021**, *11*, 1699.

3.1.2 Thermal Measurements of TIMs

Thermal properties of the prepared non-cured graphene TIMs without the copper plates were measured first. Figure 3.2 (a-b) presents the total thermal resistance of graphene TIM, R_{tot}, as a function of BLT for different graphene loading, ξ. Figure 3.2 (a) also presents

the thermal resistance of the silicone oil base polymer as a reference. Figure 3.2 (b) shows the data acquired for the graphene loading of 10 wt. % and higher for better analysis. The total thermal resistance increases linearly with as expected from previous published work [110,111]. The data were used to plot a linear regression fitting for each loading fraction as shown. For each fitting, the inverse of the line slope allowed to measure the bulk thermal conductivity of the TIM itself. The y-intercept of the fitted lines is the thermal contact resistance, R_C, of each TIM with the contact surface.

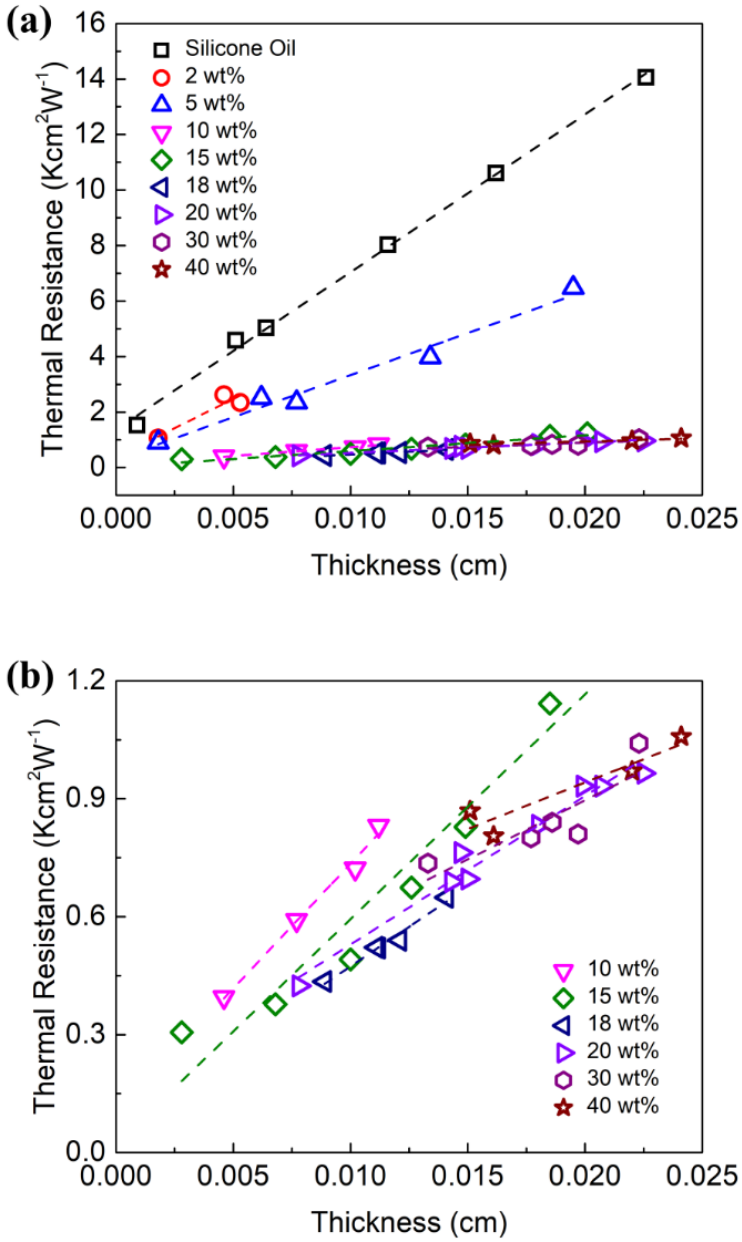

Figure 3.2: Total thermal resistance, R_{tot}, of graphene TIMs as a function of the bond line thickness, BLT. (a) Thermal resistance *vs*. BLT for all tested loading fractions of graphene fillers and pure silicone oil base. (b) Thermal resistance *vs.* BLT for loading fractions of $\xi = 10$ wt. % and more. Adapted from Ref. [20]: Sudhindra, S.; Kargar, F.; Balandin, A.A. Noncured Graphene Thermal Interface Materials for High-Power Electronics: Minimizing the Thermal Contact Resistance. *Nanomaterials* **2021**, *11*, 1699.

Figure 3.3 shows the thermal conductivity of the prepared non-cured graphene TIMs as a function of graphene loading, ξ. The thermal conductivity of the base polymer of silicone oil was measured to be $0.18\ \mathrm{Wm^{-1}K^{-1}}$. The thermal conductivity is shown to increase rapidly with the introduction of graphene fillers to the base polymer. A super-linear increase is seen suggesting that the introduced graphene fillers form a percolated network which would facilitate heat conduction. At a filler loading of $\xi = 10\ \mathrm{wt.\%}$, the increase in thermal conductivity is seen to slow down. This trend is consistent with a prior reported study for non-cured graphene TIMs [69], and different from that previously observed in curing epoxy TIMs with graphene fillers [24,25,67,89,93–95,99]. In solid cured TIMs, the thermal conductivity would reveal a linear to super-linear dependence on the loading of fillers [93]. The non-curing TIMs, on the other hand, exhibit a saturation effect for the thermal conductivity. This is similar to the previously effect for nano-fluids and soft TIMs [110–115]. The saturation effect in Figure 3.3 can be explained by the tradeoff between the enhancement trend in the thermal conductivity as more fillers are added to the base polymer matrix and the decrease in the thermal conductance due to the increase in thermal interface resistance between the filler – filler and filler – matrix interfaces as more fillers are incorporated into the polymer matrix [69]. In the studied non-cured TIMs, a thermal conductivity of $\sim 4.2\ \mathrm{Wm^{-1}K^{-1}}$ was achieved at the graphene filler loading of $40\ \mathrm{wt.\%}$. Loading fractions of above 40 wt% was not performed intentionally due to a possible issue of agglomeration. Overall, the thermal conductivity of studied graphene filler TIMs increased by the factor of ~19× and 24× for $30\ \mathrm{wt.\%}$ and $40\ \mathrm{wt.\%}$ loadings respectively compared to the thermal conductivity of the silicone oil base.

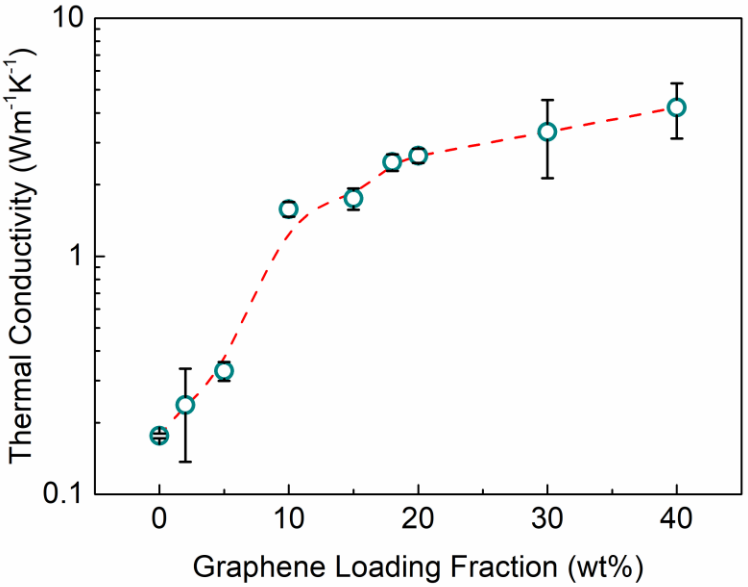

Figure 3.3: Thermal conductivity of studied non-cured TIMs as a function of graphene loading fraction, ξ. The bars at each loading fraction show the standard error of the linear regression slope. Adapted from Ref. [20]: Sudhindra, S.; Kargar, F.; Balandin, A.A. Noncured Graphene Thermal Interface Materials for High-Power Electronics: Minimizing the Thermal Contact Resistance. *Nanomaterials* **2021**, *11*, 1699.

In Figure 3.4, the measured thermal contact resistance of the studied TIMs, R_C, of each TIM as a function of graphene loading, ξ are presented. The measured dependence of $R_C(\xi)$ revealed a rather unexpected non-monotonic trend. Contrary to the expectation of increasing R_C with higher filler loading, a rapid decrease in R_C values up to the loading $\xi = 15$ wt. % can be observed, which is followed by a slow increase at the higher loading fractions of graphene fillers. Theoretically, R_C would depend on the bulk thermal conductivity and shear modulus of the TIM along with the roughness of the adjoining surfaces and the applied pressure. There would be a trade-off between the thermal

conductivity and the effect of shear modulus on R_C. The higher the thermal conductivity, the lower the R_C would be, while for the shear modulus would reveal an opposite dependence [114]. Ideally, one would want to increase the loading of fillers to improve the thermal conductivity as long as the viscosity and the shear modulus requirements would allow for it. Based on the measured dependence of $R_C(\xi)$, one would prefer to limit the loading of fillers to smaller fraction to minimize R_{tot}. One should also note that by increasing ξ, the minimum attainable BLT would be limited.

Assuming that the "bulk" thermal conductivity of the TIM layer (BLT) in semi-solid or semi-liquid TIMs would be much smaller than that of the binding surfaces, the contact resistance of a TIM can be described using the semi-empirical model [112,116,117]:

$$R_{C1+C2} = 2R_C = c\left(\frac{S_q}{K_{TIM}}\right)\left(\frac{G}{P}\right)^n. \tag{3.1}$$

where $G = \sqrt{G'^2 + G''^2}$. Here, G' and G'' are considered to be the storage modulus and the loss shear modulus of the TIM, P is the applied pressure, S_q is the average roughness of the two binding surfaces, and c and n are empirical coefficients, respectively. The two parameters would have opposite effects on the contact resistance, R_C, at a constant applied pressure. Thus, increasing the graphene filler loading would result in an increase in both thermal conductivity and G of the TIM layer (BLT). Equation 3.1 also suggests that for TIMs with a specific filler, there would exist an optimum filler loading where the thermal conductivity would increase significantly thereby slightly effecting the thermal contact resistance.

One can write the total thermal resistance from equation 3.1 as:

$$R_{tot} = \left(\frac{1}{K_{TIM}}\right)\left\{BLT + cS_q\left(\frac{G}{P}\right)^n\right\}. \tag{3.2}$$

In this form, the equation clearly indicates that an increase in the thermal conductivity of the TIM, there would be a reduction in the total thermal resistance.

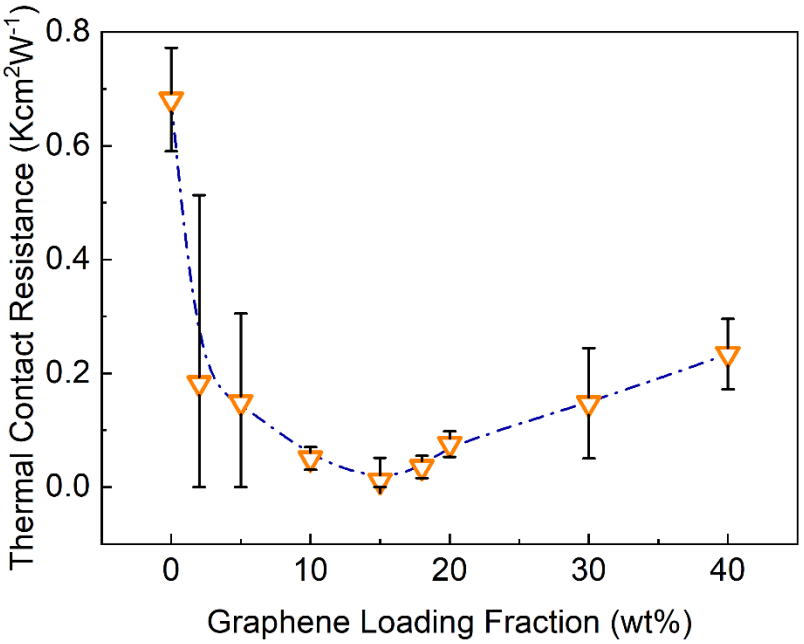

Figure 3.4: Thermal contact resistance measured TIMs as a function of the graphene loading, ξ. The bars at each loading fraction shows the standard error of the linear fittings used for data extraction. Adapted from Ref. [20]: Sudhindra, S.; Kargar, F.; Balandin, A.A. Noncured Graphene Thermal Interface Materials for High-Power Electronics: Minimizing the Thermal Contact Resistance. *Nanomaterials* **2021**, *11*, 1699.

In order to investigate the influence of the surface roughness on the thermal contact resistance of graphene filler TIMs, the total thermal resistance, R_{tot}, the as prepared copper plates were used in the TIM tester. The TIMs were placed between the TIM tester's heat

sink and source plates which are made of very flat steel plates. A fraction of a droplet of the base polymer of silicone oil was added between the top and bottom copper plates with the heat sink and source to minimize the contact resistance between the solid-solid interfaces that would originate. It is important to note that in this case, the total thermal resistance, assuming a one-dimensional heat transport would be:

$$R_{tot} = BLT/K_{TIM} + 2\left(R_{C,St-oil} + R_{C,oil-Cu} + L_{oil}/K_{oil} + L_{Cu}/K_{Cu} + R_{C,TIM-Cu}\right). \quad (3.3)$$

In equation 3.3, R_C is the thermal contact resistance between various interfaces defined by its subscripts. L and K are considered to be the thickness and bulk thermal conductivity of different components. The mentioned subscripts "St", "Cu", "oil", and TIM, represent the steel (the heat source and sink), copper plates, silicone oil, and TIM layer, respectively. It's evident that an increase in surface roughness would require more TIM to fill the air gaps on the surfaces, thus resulting in larger $R_{C,TIM-Cu}$. The interaction of the TIM layer with the surface of the plates might also change due to undulations on the surface. For the surface roughness study, TIMs with a loading fraction, ξ, of 15 wt. % and 30 wt. % were chosen. These TIMs were selected since at $\xi = 15$ wt. %, the minimum R_C is attained while $\xi = 30\ wt.\%$ would provide a trade-off between the contact resistance and thermal conductivity.

In Figure 3.5, the results of the total thermal resistance, R_{tot}, of non-cured graphene filler TIMs dispersed between two copper plates as a function of TIM's BLT for two chosen graphene loadings, ξ, and four different degrees of roughness, S_q are presented. As expected, for all the roughness values of copper plates and filler loadings, R_{tot} increases with increase in BLT. This implies that the applied TIMs were dispersed properly without

the presence unfilled air gaps due to surface roughness. An interesting observation is that in some cases, the proper selection of BLT and graphene loading, ξ, would compensate for increase in the surface roughness, S_q. This can be noticed in the case of the chosen TIM with a loading fraction of 30 wt. % of graphene fillers and two roughness values of 1.2 μm and 3.1 μm. It is interesting to note that the use of a BLT ~300 μm with the copper plates that were characterized by larger values of surface roughness, $S_q = 3.1$ μm, did not result in the overall increase in R_{tot} as compared to the copper plates with $Sq = 1.2$ μm.

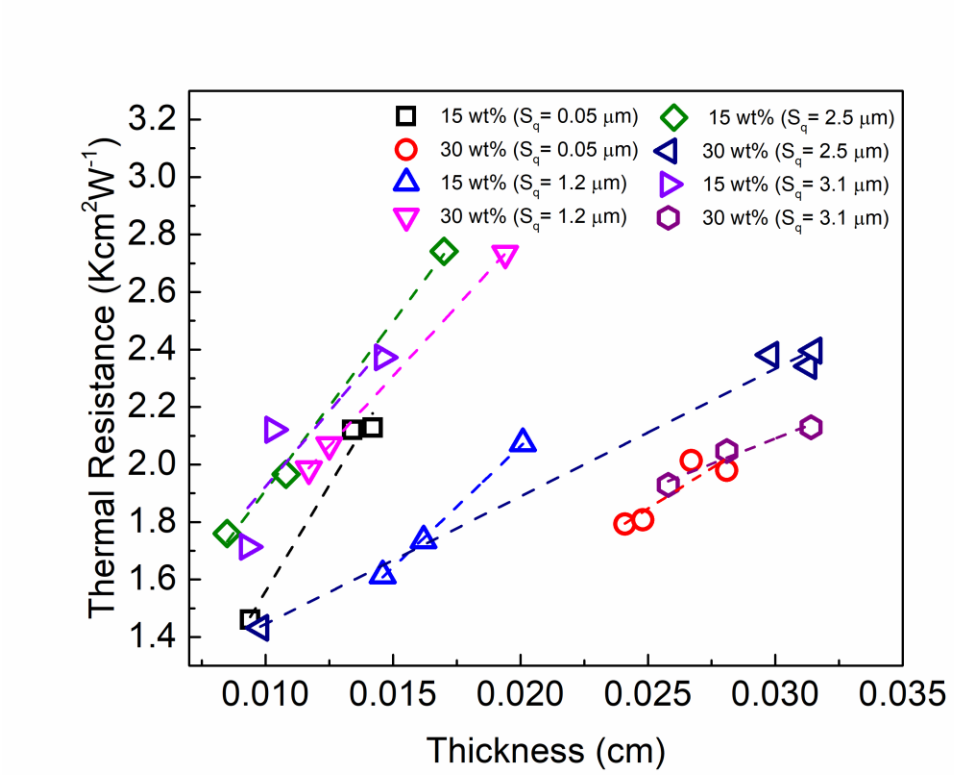

Figure 3.5: Thermal resistance, R_{tot}, of the graphene TIM dispersed between two copper plates as a function of the bond line thickness, BLT. The results are presented for two different graphene loadings, ξ, and four different values of roughness, S_q. In each measurement, the two copper plates used had the same roughness. The dashed lines show the linear regression fittings to the experimental data. Adapted from Ref. [20]: Sudhindra, S.; Kargar, F.; Balandin, A.A. Noncured Graphene Thermal Interface Materials for High-Power Electronics: Minimizing the Thermal Contact Resistance. *Nanomaterials* **2021**, *11*, 1699.

The extracted thermal contact resistance, R_C, from each linear regression fittings of each data set presented in Figure 3.5. According to the equation 3.3, the sandwiched TIMs between the copper plates, the *y*-intercept of the plot would be $2(R_{C,St-oil} + R_{C,oil-Cu} + L_{oil}/K_{oil} + L_{Cu}/K_{Cu} + R_{C,TIM-Cu})$. The thermal resistance of the copper plates is considered to be negligible and considered to be ($2L_{Cu}/K_{Cu} \sim 7.3 \times 10^{-4}$ °Ccm^{2}W^{-1}). Thus, the *y*-intercept would in fact present the summation of the total

contact resistance of the measured sandwich structure $R_C = 2(R_{C,St-oil} + R_{C,oil-Cu} + R_{C,TIM-Cu})$ plus the thermal resistance of the silicone oil layer at the copper-TIM tester plate interfaces ($R_{oil} = L_{oil}/K_{oil}$).

In each measurement, the $R_{C,St-oil}$, $R_{C,oil-Cu}$, and L_{oil}/K_{oil} would be considered as fixed values since the surface roughness of all the utilized copper plates at the interfaces with the heat source and sink plates and the thickness of the oil layer are the same. Thus, the extracted values for the $R_C + R_{oil}$ shown in Figure 3.6 indicates a parameter for measuring the contact resistance between the TIM layer and varying surface roughness of the copper plates. The determined values of contact resistance as a function of the surface roughness is shown in Figure 3.6. The thermal contact resistance is shown to increase with the surface roughness. The contact resistance for TIM with the higher loading of 30 wt. %, is larger than that with a loading of 15 wt. % as expected due to the performance of silicone oil based non-cured TIMs.

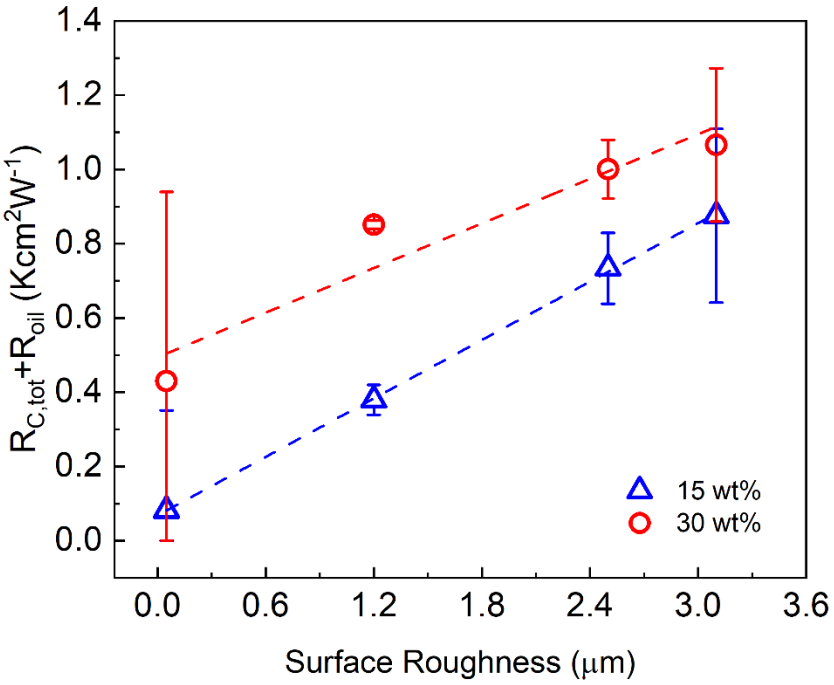

Figure 3.6: Thermal contact resistance ($R_{C,tot} + R_{oil}$) of graphene TIMs introduced between two copper plates as a function of the surface roughness. Adapted from Ref. [20]: Sudhindra, S.; Kargar, F.; Balandin, A.A. Noncured Graphene Thermal Interface Materials for High-Power Electronics: Minimizing the Thermal Contact Resistance. *Nanomaterials* **2021**, *11*, 1699.

In high power electronic packaging, a non-cured TIM is ideally applied between the direct bond copper (DBC) layer and the heat sink [118–121] and usually, this layer is the bottleneck of the design of packaging as the thermal resistance of TIM is usually the highest among the other constituent components. Thus, there have been previous efforts on decreasing the thermal resistance of the TIM layer by improving the bulk thermal conductivity of the TIM and also by reducing the BLT at the interface. By reducing the thickness of the BLT layer, the effect of the thermal contact resistance and surface roughness of the adjoining surfaces would become more dominant. Recent efforts towards

application of diamond-based electronics has shown improvement of the heat transport at the device level due to the high thermal conductivity of diamond. However, it still lacks proper treatment and dissipation of the generated heat at the system and packaging level where the high surface roughness of the diamond-based devices would become problematic. The results presented in this study implies that the change of surface roughness in the scale of ~1 μm substantially would increase the thermal contact resistance by a factor of ×2 and thus, should be addressed properly in the process of packaging. The presented results would also suggest that graphene-based TIMs with optimized filler loading can be considered as a potential solution for high-power electronics because of their improved thermal conductivity and also its low thermal contact resistance.

3.2 Results and Discussions

3.2.1 Characterization of Graphene Filler Size

For the filler size study, the prepared non-cured silicone oil-based graphene and FLG filler TIMs were produced from graphite using the liquid phase exfoliation (LPE) technique [122–126] in an aqueous surfactant solution with a combination of liquid cascade centrifugation [127,128] for size selection of fillers as explained in section 2.2.3. This procedure enabled the production of three fractions from the same stock dispersion with different distributions of lateral size and thickness. The exfoliated graphene fillers were then extracted from it's solvent and were incorporated with the base polymer to produce the required TIMs according the procedure explained in section 2.3.2. The characterization of these graphene fillers for lateral dimension and thickness (number of layers) was

essential for the study and was performed with the help of the technique of atomic force microscopy (AFM). To assess the concentration/mass, optical extinction spectroscopy was used. In Figure 3.7, the characterization data of AFM for the three size sets of graphene fillers are presented. Figure 3.7 (a-c) presents the two-dimensional AFM images of the dispersed graphene fillers in fractions of size selection. The histograms of the AFM measurements for the longest dimension of graphene fillers (L) are presented in Figure 3.7 (d-f) while the histograms from AFM measurements for the number of atomic planes (N) are presented in Figure 3.7 (g-i). It is essential to note that due to the log-normal shape of the graphene filler distributions, there are multiple ways to describe the average characteristic values of them. Here, the focus is on the arithmetic mean of the graphene filler dimensions which were calculated to be 1200 nm, 800 nm and 400, while the average number of atomic planes of graphene fillers were determined to be 40, 19 and 8 for large, medium and small fillers respectively. For the ease of understanding, these fillers have been labelled as “large”, “medium” and “small”.

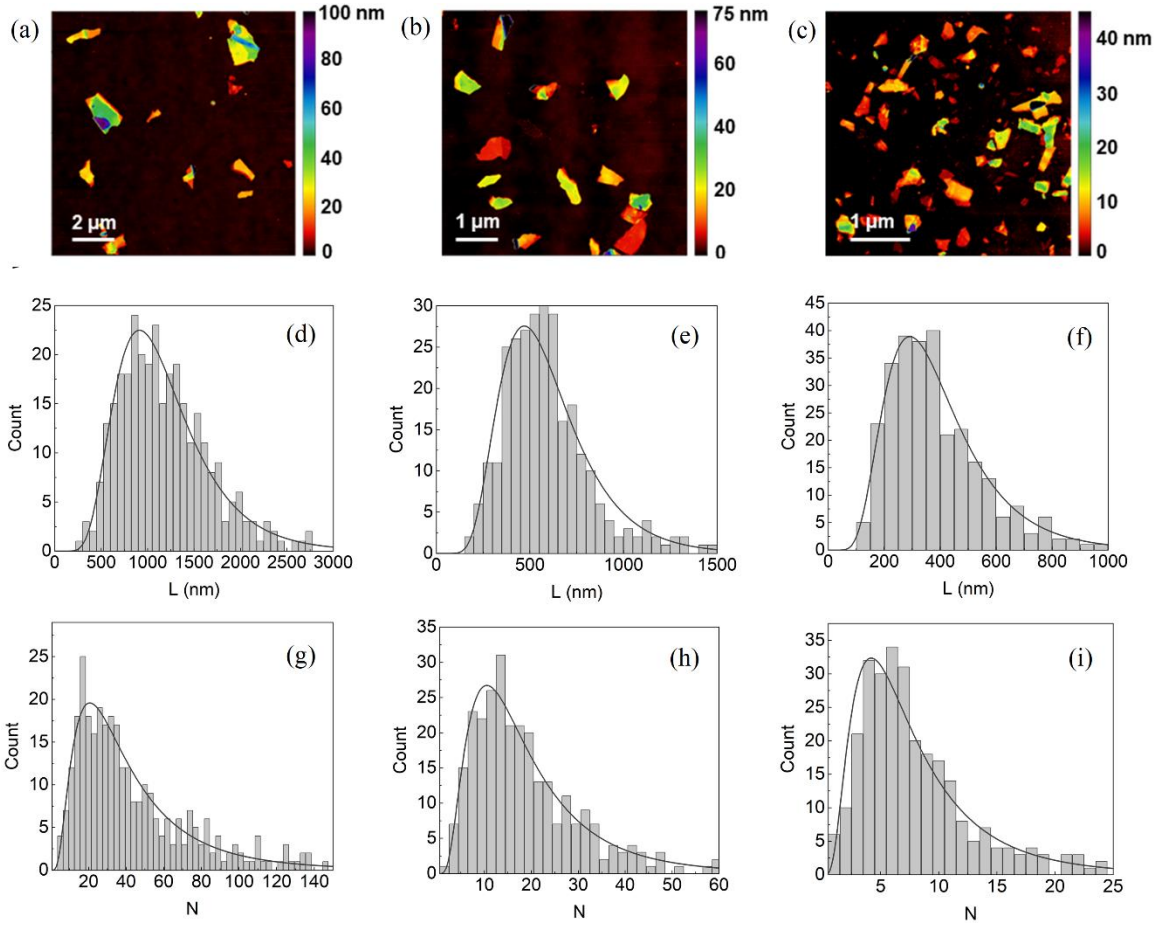

Figure 3.7: Characterization of graphene fillers with AFM. (a–c) Two-dimensional images of the large, medium and small size graphene fillers, respectively. These fillers were drop-casted on a Si/SiO_2 substrate for the measurements. (d-f) Histograms of the measured graphene filler lengths that were used for determining the filler sizes using AFM. (g-i) Histograms of the number of atomic planes of the graphene fillers with the help of AFM. Adapted from Ref. [129]: Sudhindra, S.; Rashvand, F.; Wright, D.; Barani, Z.; Drozdov, A.D.; Baraghani, S.; Backes, C.; Kargar, F.; Balandin, A.A. Thermal Transport in Graphene Composites: The Effect of Lateral Dimensions of Graphene Fillers. *Archive* **2021**, 1–38.

One should note that there is a correlation between the lateral dimensions and the number of atomic planes in the FLG fillers. Practically, obtaining FLG fillers with a fixed number of atomic planes and different lateral dimensions is difficult. This is due to the mechanism of exfoliation which can be described in terms of delamination along with

tearing [130]. The centrifugation, process which is required for the size selection, would enhance this correlation and would typically produce the small graphene fillers that are thinner and the large graphene fillers that are thicker [127,130]. This correlation can be explained with a plot of the area of fillers as function of number of the atomic planes of the graphene fillers. Figure 3.8 (a) presents the characteristic lateral length, $L_* = (L \times W)^{0.5}$ as a function of the number of atomic planes represented as N (L and W are considered to be the measured "length" and "width" of the graphene fillers acquired from AFM measurements). In this plot, each data point would correspond to a every graphene sheet measured with AFM during the size selection fractions process. The acquired specifications of the graphene fillers acquired from the AFM measurements are presented in Table 3.1. For the FLG fillers, the lateral dimensions would affect the thermal transport stronger than the thickness [61,78,79,90,131–135]. Thus, the prepared sets TIMs are useful for understanding the importance and specifics heat conduction and the effects of the graphene filler size.

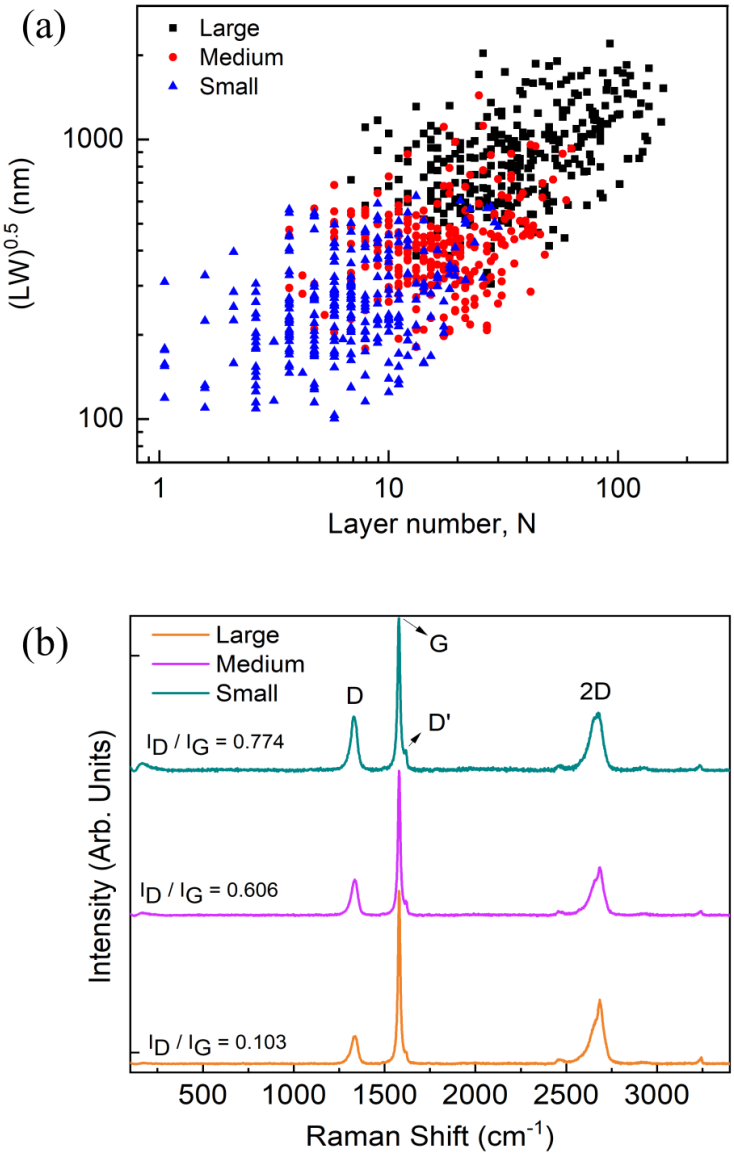

Figure 3.8: (a) Correlation between the measure of the lateral dimensions of the graphene fillers and the number of the atomic planes of the graphene fillers. The multiple data points denote the numerous measurements conducted with the AFM. (b) Raman spectra of different lateral dimensions of graphene fillers. Adapted from Ref. [129]: Sudhindra, S.; Rashvand, F.; Wright, D.; Barani, Z.; Drozdov, A.D.; Baraghani, S.; Backes, C.; Kargar, F.; Balandin, A.A. Thermal Transport in Graphene Composites: The Effect of Lateral Dimensions of Graphene Fillers. *Archive* **2021**, 1–38.

The quality of graphene fillers using Raman spectroscopy (Renishaw inVia) to ensure the difference in size of the fillers. Figure 3.8 (b) presents the measured Raman spectra of the three sets of graphene fillers used in this study. In order to conduct the necessary tests, a small portion of each graphene fillers were transferred onto a Si/SiO_2 substrate. The process of light scattering spectra were collected under a laser excitation of the wavelength 633 nm (red) and an excitation power of 2 mW at room temperature. The Raman spectra displayed well-known signatures of FLG, which are the G peak and 2D band [128,132,133,136–138]. As per expectation, the intensity of the disorder D peak increased as the size of the graphene fillers decreased. These evolution of the peaks with the lateral dimensions and the number of the atomic planes is in line with prior conducted work from various researchers [136,137,139–141]. The I_D/I_G ratio of the Raman spectra can be qualitatively used to explain the difference in the average size of the fillers [142]. The I_D/I_G ratio was measured and it decreased as the size of the graphene fillers increased as shown in the plot. The evolution of the D peak and I_D/I_G can be described by the relaxation of the selection rules, which prohibit the appearance of the D peak in graphene with perfect translation symmetry, without defects or edges [143,144]. In the smaller graphene fillers, the excitation laser light would cover more graphene fillers with the edges that would act as inherent defects thus resulting in an increase in the I_D/I_G ratio. The 2D peak becomes more symmetric with the decrease in filler dimensions which is in this case due to the number of atomic planes. However, as recorded recently, this factor cannot be used as quantitative measure for the thickness in LPE of graphene [145].

Table 3.1: Characteristics of exfoliated Graphene – FLG Fillers as a result of AFM measurements.

	Symbol	**Large**	**Medium**	**Small**
Average length (nm)	L	1200	600	400
Aspect ratio (length/width)	L/W	1.8	2.1	2.3
Aspect ratio (length/thickness)	(L/t)	110	120	200
Average layer number	N	40	19	8
Characteristic length $(L \times W)^{0.5}$ (nm)	L_*	900	430	270

3.2.2 Thermal Measurements of TIMs

The bulk thermal characteristics of the prepared TIMs with different filler sizes were also measured using the TIM tester described in the previous chapter. The testing specifications were similar to the roughness project but the only difference being in not using the rough copper plates. The total thermal resistance, R_{tot}, of the prepared non-cured graphene TIMs as a function of its BLTs is shown in Figures 3.9, 3.10 and 3.11. The data are presented for all three chosen lateral dimensions of the graphene fillers at different loading fractions (*f*) in vol%.

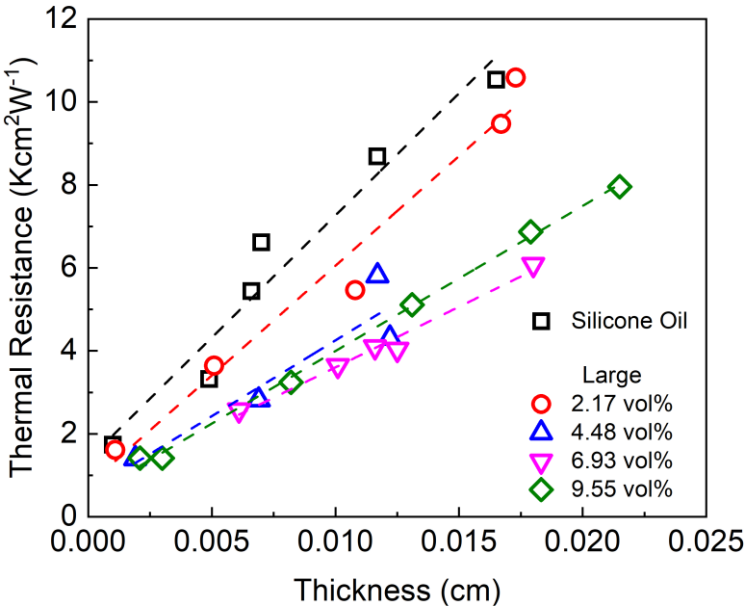

Figure 3.9: Total thermal resistance of the large filler size graphene TIMs as a function of BLT. Adapted from Ref. [129]: Sudhindra, S.; Rashvand, F.; Wright, D.; Barani, Z.; Drozdov, A.D.; Baraghani, S.; Backes, C.; Kargar, F.; Balandin, A.A. Thermal Transport in Graphene Composites: The Effect of Lateral Dimensions of Graphene Fillers. *Archive* **2021**, 1–38.

As per expectation, the total thermal resistance is shown to increase linearly with BLT. The acquired data for each filler size and each loading fraction were used to plot a linear regression fitting. It can clearly be seen that the thermal resistance at constant thickness is the highest for the polymer material of silicone oil without the addition of graphene fillers.

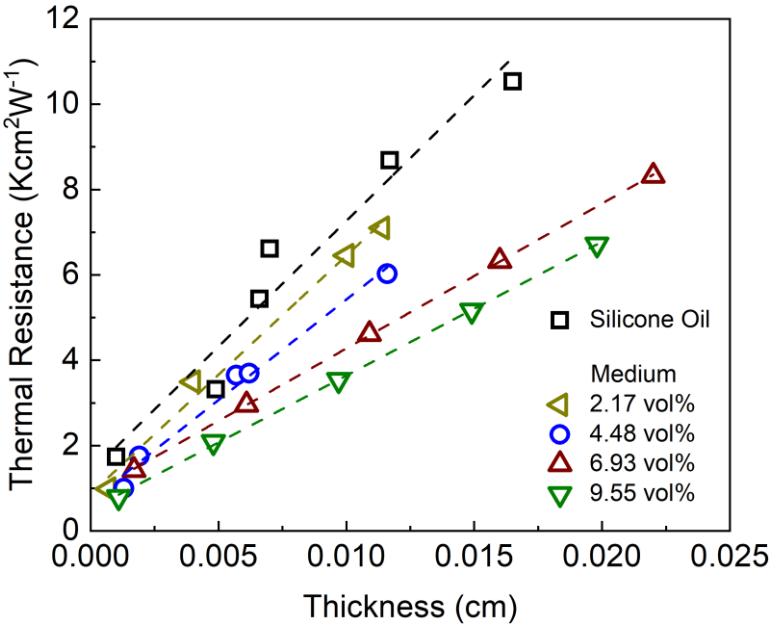

Figure 3.10: Total thermal resistance of the medium filler size graphene TIMs as a function of BLT. Adapted from Ref. [129]: Sudhindra, S.; Rashvand, F.; Wright, D.; Barani, Z.; Drozdov, A.D.; Baraghani, S.; Backes, C.; Kargar, F.; Balandin, A.A. Thermal Transport in Graphene Composites: The Effect of Lateral Dimensions of Graphene Fillers. *Archive* **2021**, 1–38.

The contact resistance is the lowest for the TIMs with the higher loading fraction of graphene fillers. However, it is difficult to draw conclusions about the effect of the graphene filler size from this plot. But, the latter is possible in a meaningful way from the analysis of the thermal conductivity and contact resistance of the TIMs.

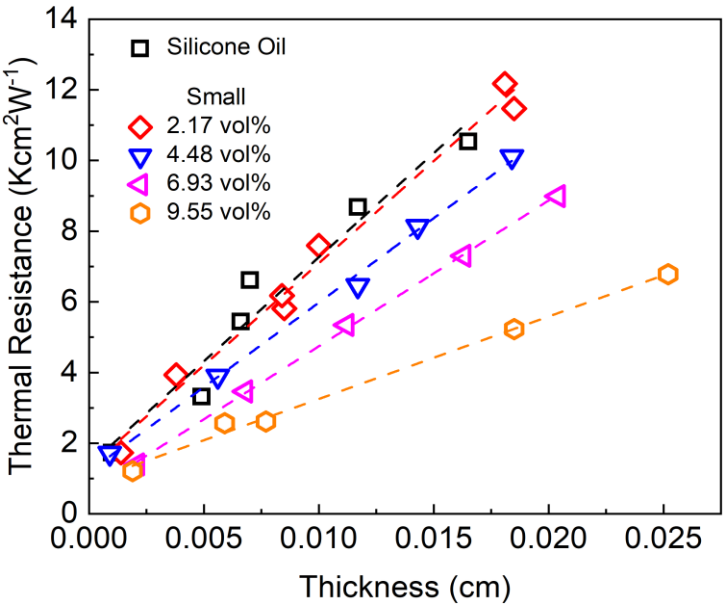

Figure 3.11: Total thermal resistance of the small filler size graphene TIMs as a function of BLT. Adapted from Ref. [129]: Sudhindra, S.; Rashvand, F.; Wright, D.; Barani, Z.; Drozdov, A.D.; Baraghani, S.; Backes, C.; Kargar, F.; Balandin, A.A. Thermal Transport in Graphene Composites: The Effect of Lateral Dimensions of Graphene Fillers. *Archive* **2021**, 1–38.

Figure 3.12 shows the thermal contact resistance of the prepared and tested TIMs with different filler sizes as a function of graphene filler loading fraction. The plot can be explained with the same concept used to explain the contact resistance plot in the surface roughness project while analysing the contact resistance of the TIMs without the rough copper plates. To explain the effect of the filler size on contact resistance, it is essential to understand the role of G' and G'' on the viscosity of the TIMs and ultimately the issue of "pump-out" [19,69,120,146]. There have been multiple reported studies on the influence of G' and G'' in composites of varying filler sizes [147–156] and it has been documented that G' and G''would decrease as the size of the filler increases. Here, it is essential to note that viscosity of the base polymer also plays an important role in determining G' and G''

and, ultimately, explaining the effect of pump-out [23,157,158]. It has been suggested in a previous study [117] that G' of a TIM should be greater than G'' in order to avoid the pump-out issue.

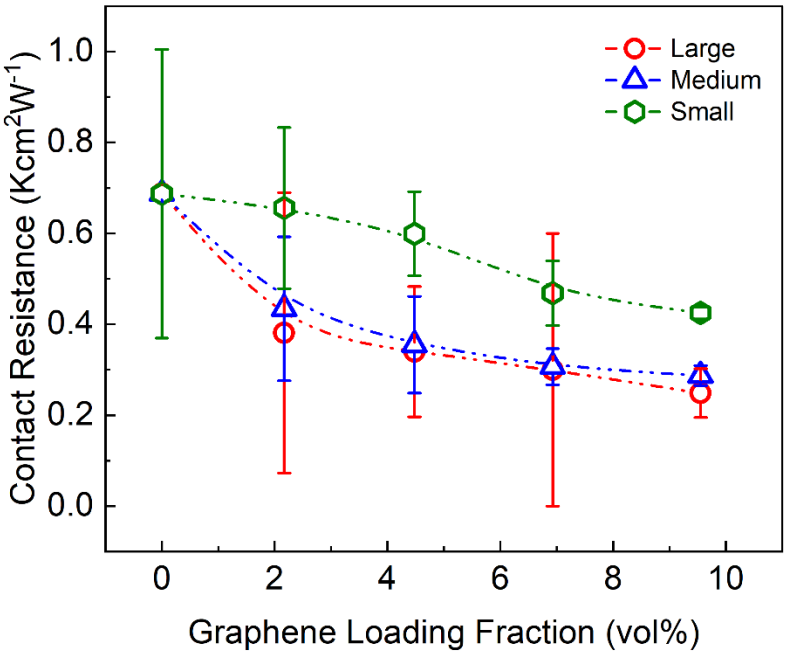

Figure 3.12: Contact resistance of the studied TIMs as a function of the graphene loading fraction (vol%). The error bars show the standard error obtained from the linear regression fittings. Adapted from Ref. [129]: Sudhindra, S.; Rashvand, F.; Wright, D.; Barani, Z.; Drozdov, A.D.; Baraghani, S.; Backes, C.; Kargar, F.; Balandin, A.A. Thermal Transport in Graphene Composites: The Effect of Lateral Dimensions of Graphene Fillers. *Archive* **2021**, 1–38.

In Figure 3.13, the experimental measured thermal conductivity as a function of graphene loading fraction for the studied graphene filler sizes and a comparison with a theoretical model is presented. The thermal conductivity is shown to slightly increase till a

loading fraction of $f = 2.17$ vol. % and then shown to linearly increase faster. The thermal conductivity of the TIMs is higher for the large graphene filler size for all the measured loading fractions. It can clearly be seen that in the studied range of the lateral dimensions of the graphene fillers, the thermal conductivity of the TIMs increases with increase in the size of the graphene fillers. This trend can be rationalized with the comparison of the size of the graphene fillers with the average, also known as *gray,* phonon MFP in graphene. The gray phonon MFP in graphene is reported to be in the order of ~800 nm at room temperature [78,79,132,133,135,159]. The improvement in the thermal conductivity of the studied TIMs stems from thermal transport, which happens, at least partially, via the graphene fillers. If the filler lateral dimensions become smaller than the phonon MFP its own thermal conductivity would decrease. The simple estimate arises from the Debye model, where the thermal conductivity $K \sim Cv\Lambda$ (here C is considered to be specific heat, v is considered to be the average phonon group velocity and Λ as the average phonon MFP). When the size of the filler is considered to be $L < \Lambda$, then, the thermal conductivity (K) would scale down linearly with lateral dimension (L). This explanation would remain valid for the thermal transport regime below and above the thermal percolation threshold [67].

In order to better explain the effect of filler loading on thermal conductivity of a polymer composite (TIM) in Figure 3.13, the Kanari model [160] was implemented which was introduced as an empirical extension of the Bruggerman relation [161]. The derivation of the Kanari model within the micromechanical framework was previously explained in detail [162]. According to this approach, the thermal conductivity of a composite consisting

of a polymer matrix reinforced with particles of an arbitrary shape is determined by the equation:

$$\frac{k_f - K_{TIM}}{k_f - k_m}\left(\frac{k_m}{K_{TIM}}\right)^{\frac{1}{B}} = 1 - f. \tag{3.4}$$

Where k_m, k_f are the thermal conductivities of the polymer matrix and filler, respectively while f is the volume fraction of fillers and B stands for a parameter characterizing shape of the filler particles. These stacks of graphene plates are treated as oblate ellipsoids of rotation with semi-axes $a_1 < a_2 = a_3$, where a_1 is the characteristic thickness of a stack while $a_2 = a_3 = L_*$ is its in-plane size. Under this condition and given for a fact that $k_f \gg k_m$, the coefficient B can be represented as:

$$B = \frac{4 - 3M}{3M(1 - M)} \tag{3.5}$$

With,

$$M = \frac{2\varphi - \sin\varphi}{2sin^2\varphi}\cos\varphi, \qquad \cos\varphi = \frac{a_1}{a_2} \tag{3.6}$$

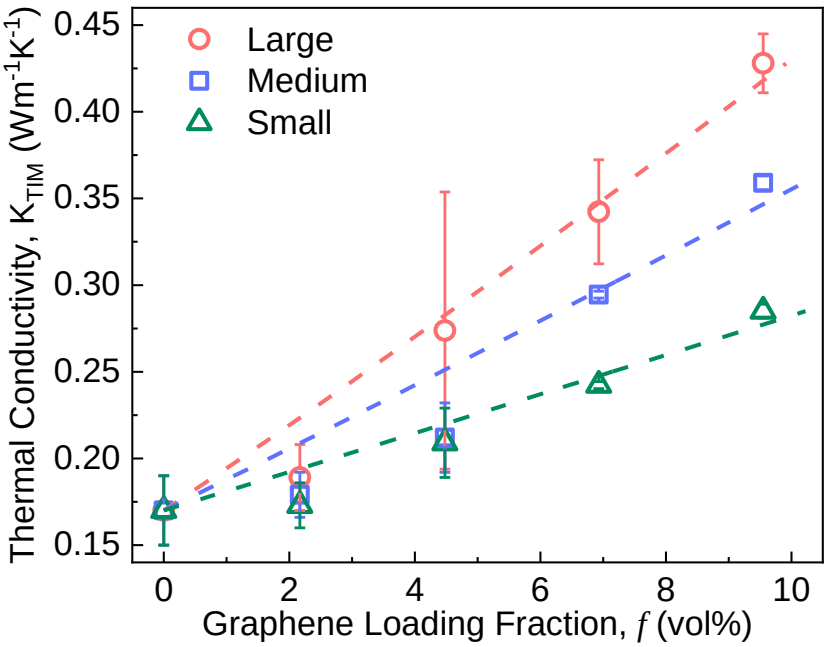

Figure 3.13: Experimentally acquired thermal conductivity data (symbols) of the studied non-cured TIMs as a function of the graphene loading fraction, f, for the studied three different sizes of the fillers with theoretical comparison of the Kanari model (dashed lines). Adapted from Ref. [129]: Sudhindra, S.; Rashvand, F.; Wright, D.; Barani, Z.; Drozdov, A.D.; Baraghani, S.; Backes, C.; Kargar, F.; Balandin, A.A. Thermal Transport in Graphene Composites: The Effect of Lateral Dimensions of Graphene Fillers. *Archive* **2021**, 1–38.

Figure 3.13 presents a reasonable agreement between the experimental data of TIMs with small, medium and large graphene fillers and the theoretical modeling. Each set of data is separately a function of its parameter, the effective thermal conductivity of the fillers k_f. In simulation, the value $k_m = 0.17\ \mathrm{Wm^{-1}K^{-1}}$ for thermal conductivity of the polymer matrix is adopted. The coefficients φ, M, and B, related to the aspect ratio of fillers, are calculated based on the experimental characterization of the fillers as presented in Table 3.1 and their values are summarized in Table 3.2.

Table 3.2: Simulation parameters used in Kanari model.

Filler Type	Layer Number (N)	thickness (a_1)[nm]	Plane dimension ($a_2 = a_3 = L_*$)[nm]	φ [rad]	M	B
Large	40	14	900	1.5552	0.0164	81.5419
Medium	19	6.65	430	1.55533	0.0163	82.0100
Small	8	2.8	270	1.56043	0.0110	121.5660

The influence of the in-plane size of fillers on their effective thermal conductivity k_f is presented in Figure 3.14 as a function L_* and with an approximation of the data with an exponential function:

$$k_f = k_f^0 + k_f^1 \exp(-\alpha L_*). \quad (3.7)$$

where $k_f^0 = 3.32$, $k_f^1 = -4.83$, and $\alpha = 0.0033$ are fitting parameters. Figure 3.12 clearly illustrates that k_f increases by a factor of 2.2 with L_* when the in-plane size of the fillers increases from 270 to 900 nm. The theoretically extracted effective thermal conductivity of fillers is orders of magnitude smaller than the intrinsic thermal conductivity of graphene because of the filler-polymer thermal boundary resistance. However, the decrease in the effective thermal conductivity of the fillers as their size shrinks below graphene's phonon MFP is originated from a strong suppression of the its intrinsic thermal conductivity due to the enhanced phonon-edge scattering.

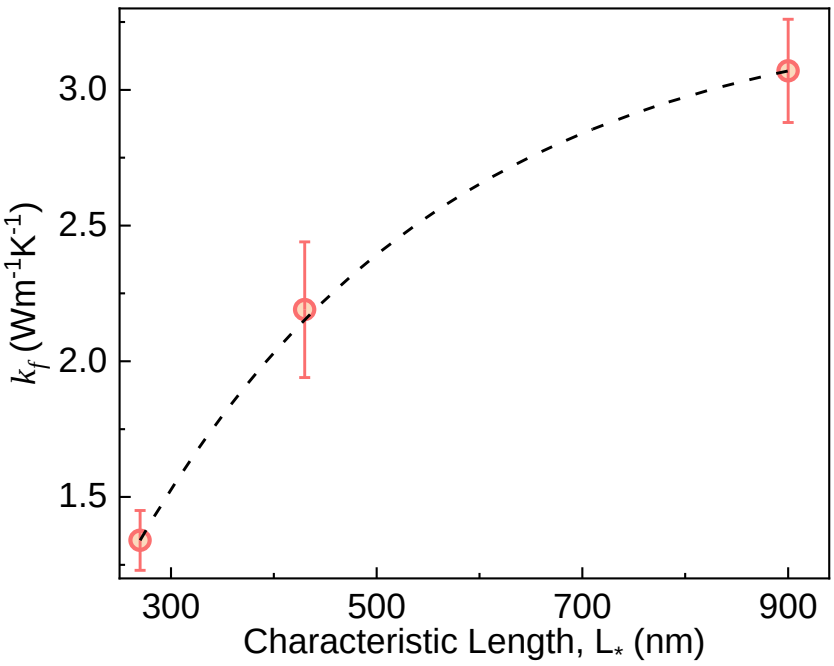

Figure 3.14: Effective thermal conductivity of filler k_f versus the characteristic in-plane size of graphene fillers L_*. Adapted from Ref. [129]: Sudhindra, S.; Rashvand, F.; Wright, D.; Barani, Z.; Drozdov, A.D.; Baraghani, S.; Backes, C.; Kargar, F.; Balandin, A.A. Thermal Transport in Graphene Composites: The Effect of Lateral Dimensions of Graphene Fillers. *Archive* **2021**, 1–38.

The presented study implies that a stronger enhancement of the thermal conductivity of graphene composites can be achieved when the fillers with larger lateral dimensions are utilized. This realization is in line with previously reported studies [44–46,93,163–165]. The prior studies were conducted on substantially larger fillers dimensions of above 5 μm. In many cases, no accurate assessment and averaging were performed for the size distribution of the fillers used in the previously reported studies. Thus, due to the selection of the average filler sizes near the phonon MFP of graphene, *i.e.*, slightly smaller, almost equal, and slightly larger, this study was able to connect the studied trend with the intrinsic heat conduction properties of FLG. The observation that the thermal

contact resistance also decreases with increasing the graphene filler size is a non-obvious trend, and to some degree, counter-intuitive as well. The presented trends throw light on the importance of heat conduction in graphene composites and TIMs, and can be utilized for optimization for its practical applications.

3.3 Conclusions

In this thesis, I first reported on investigation of the thermal contact resistance of the non-cured graphene TIMs with surfaces of various degrees of roughness. It was realized that the thermal contact resistance of the TIMs would depend on the graphene loading non-monotonically while achieving its minimum at the loading fraction of ~ 15 wt. % for the studied graphene filler TIMs. Increasing the surface roughness by 1 μm would result approximately in the factor of ×2 increase in the thermal contact resistance of the studied TIMs. The total thermal resistance of the layer of the non-cured TIMs would scale linearly with the BLT in the studies range. A projection to the micrometer BLT indicates that graphene TIMs have the potential to meet the thermal management requirements for the high-power electronics for present and future applications.

In the second part of this thesis, I reported on investigation of the thermal properties of non-cured silicone oil TIMs with graphene and FLG fillers of different lateral dimensions. The graphene fillers had lateral dimensions in the range from 400 nm to 1200 nm and number of atomic planes from one to ~100 and were labelled as “small”, “medium” and “large” respectively. In the examined range of the lateral dimensions of the graphene

fillers, the thermal conductivity of the TIMs increased with the size of the fillers. The thermal contact resistance of TIMs with graphene fillers of 1200-nm lateral dimensions was found to be smaller than that of TIMs with graphene fillers of 400-nm lateral dimensions. The influence of the filler loading fraction and the filler size on the thermal conductivity of the composites theoretically compared with the Kanari model.

The obtained results from both the research projects are essential for the optimization of graphene filler TIMs for its application in heat removal from high-power-density electronics.

References

1. Moore, G.E. Cramming More Components Onto Integrated Circuits. *Proceedings of the IEEE* **1998**, *86*, 82–85, doi:10.1109/JPROC.1998.658762.

2. Mueller, S. *Upgrading and Reparing PCs*; 17th ed.; Que, 2006;

3. Strecker, W.D. Transient Behavior of Cache Memories. *ACM Transactions on Computer Systems (TOCS)* **1983**, *1*, 281–293, doi:10.1145/357377.357379.

4. Przybylski, S.; Horowitz, M.; Hennessy, J. Characteristics of Performance-Optimal Multi-Level Cache Hierarchies. *Proceedings of the 16th Annual International Symposium on Computer Architecture* **1989**.

5. Borkar, S.; Chien, A.A. The Future of Microprocessors. *Communications of the ACM* **2011**, *54*, 67, doi:10.1145/1941487.1941507.

6. Ferain, I.; Colinge, C.A.; Colinge, J.-P. Multigate Transistors as the Future of Classical Metal–Oxide–Semiconductor Field-Effect Transistors. *Nature* **2011**, *479*, 310–316, doi:10.1038/nature10676.

7. Huang, W.; Stan, Mircea.R.; Gurumurthi, S.; Ribando, Robert.J.; Skadron, K. Interaction of Scaling Trends in Processor Architecture and Cooling. *26th Annual IEEE Semiconductor Thermal Measurement and Management Symposium (SEMI-THERM), Santa Clara, CA* **2010**, 198–204.

8. Huang, W.; Howie, J.; Taylor, A.; Robinson, N. An Investigation into the Effectiveness of Traditional Chinese Acupuncture (TCA) for Chronic Stress in Adults: A Randomised Controlled Pilot Study. *Complementary Therapies in Clinical Practice* **2011**, *17*, 16–21, doi:10.1016/j.ctcp.2010.05.013.

9. Schelling, P.K.; Shi, L.; Goodson, K.E. Managing Heat for Electronics. *Materials Today* **2005**, *8*, 30–35, doi:10.1016/S1369-7021(05)70935-4.

10. Pop, E.; Sinha, S.; Goodson, K.E. Heat Generation and Transport in Nanometer-Scale Transistors. *Proceedings of the IEEE* **2006**, *94*, 1587–1601, doi:10.1109/JPROC.2006.879794.

11. Haensch, W.; Nowak, E.J.; Dennard, R.H.; Solomon, P.M.; Bryant, A.; Dokumaci, O.H.; Kumar, A.; Wang, X.; Johnson, J.B.; Fischetti, M. v. Silicon CMOS Devices Beyond Scaling. *IBM Journal of Research and Development* **2006**, *50*, 339–361, doi:10.1147/rd.504.0339.

12. Hamann, H.F.; Weger, A.; Lacey, J.A.; Hu, Z.; Bose, P.; Cohen, E.; Wakil, J. Hotspot-Limited Microprocessors: Direct Temperature and Power Distribution Measurements. *IEEE Journal of Solid-State Circuits* **2007**, *42*, 56–65, doi:10.1109/JSSC.2006.885064.

13. Amalu, E.H.; Ekere, N.N.; Bhatti, R.S. High Temperature Electronics: R&D Challenges and Trends in Materials, Packaging and Interconnection Technology. In Proceedings of the 2009 2nd International Conference on Adaptive Science & Technology (ICAST); December 2009; pp. 146–153.

14. Cengel, Y.A. *Heat Transfer: A Practical Approach*; 2nd ed.; McGraw-Hill: New York, 2004;

15. Bar-Cohen, A.; Matin, K.; Narumanchi, S. Nanothermal Interface Materials: Technology Review and Recent Results. *Journal of Electronic Packaging* **2015**, *137*, doi:10.1115/1.4031602.

16. Bar-Cohen, A.; Matin, K.; Jankowski, N.; Sharar, D. Two-Phase Thermal Ground Planes: Technology Development and Parametric Results. *Journal of Electronic Packaging* **2015**, *137*, doi:10.1115/1.4028890.

17. Yovanovich, M.M.; Marotta, E.E. *Thermal Spreading and Contact Handbook, in Heat Transfer Handbook*; Bejan, A., Kraus, A.D., Eds.; Wiley: New Jersey, 2003;

18. Madhusudana, C. v. *Thermal Contact Conductance*; Springer-Veralag: New York, 1996;

19. Gwinn, J.P.; Webb, R.L. Performance and Testing of Thermal Interface Materials. In Proceedings of the Microelectronics Journal; March 2003; Vol. 34, pp. 215–222.

20. Sudhindra, S.; Kargar, F.; Balandin, A.A. Noncured Graphene Thermal Interface Materials for High-Power Electronics: Minimizing the Thermal Contact Resistance. *Nanomaterials* **2021**, *11*, 1699, doi:10.3390/nano11071699.

21. Holman, Jack.P. *Heat Transfer*; 9th ed.; McGraw-Hill, 2002;

22. Prasher, R.S. Surface Chemistry and Characteristics Based Model for the Thermal Contact Resistance of Fluidic Interstitial Thermal Interface Materials. *Journal of Heat Transfer* **2001**, *123*, 969–975, doi:10.1115/1.1388301.

23. Prasher, R. Thermal Interface Materials: Historical Perspective, Status, and Future Directions. *Proceedings of the IEEE* **2006**, *94*, 1571–1586, doi:10.1109/JPROC.2006.879796.

24. Shahil, K.M.F.; Balandin, A.A. Graphene-Multilayer Graphene Nanocomposites as Highly Efficient Thermal Interface Materials. *Nano Letters* **2012**, *12*, 861–867, doi:10.1021/nl203906r.

25. Shahil, K.M.F.; Balandin, A.A. Thermal Properties of Graphene and Multilayer Graphene: Applications in Thermal Interface Materials. *Solid State Communications* **2012**, *152*, 1331–1340, doi:10.1016/j.ssc.2012.04.034.

26. Fletcher, L.S. *Conduction in Solids-Imperfect Metal-to-Metal Contacts: Thermal Contact Resistance, in Heat Transfer and Fluid Mechanics Data Books*; Genium Publishing Company: Schenectady, NY, 1991;

27. Lambert, M.A.; Fletcher, L.S. Metallic Coatings for Enhancement of Thermal Contact Conductance. *Journal of Thermophysics and Heat Transfer* **1994**, *8*, 341–348, doi:10.2514/3.544.

28. Wolff, E.G.; Schneider, D.A. Prediction of Thermal Contact Resistance Between Polished Surfaces. *International Journal of Heat and Mass Transfer* **1998**, *41*, 3469–3482, doi:10.1016/S0017-9310(98)00067-2.

29. Babu, S.; Manisekar, K.; Kumar, A.P.S.; Rajenthirakumar, D. Experimental Study of Thermal Contact Resistance in Hardened Bearing Surfaces. *Experimental Heat Transfer* **2015**, *28*, 189–203, doi:10.1080/08916152.2013.860503.

30. Marotta, E.E.; Mazzuca, S.J.; Norley, J. Thermal Joint Conductance for Flexible Graphite Materials: Analytical and Experimental Study. *IEEE Transactions on Components and Packaging Technologies* **2005**, *28*, 102–110, doi:10.1109/TCAPT.2004.843153.

31. Shaik, R.A.; Beall, A.N.; Razani, A. Thermal Modeling of the Effect of Interstitial Fluid on Contact Resistance Between Two Dissimilar Materials. *Heat Transfer Engineering* **2001**, *22*, 41–50, doi:10.1080/01457630150215712.

32. Shaikh, S.; Lafdi, K.; Silverman, E. The Effect of a CNT Interface on the Thermal Resistance of Contacting Surfaces. *Carbon* **2007**, *45*, 695–703, doi:10.1016/j.carbon.2006.12.007.

33. Maisuria, M. Effect of Surface Roughness on Heat Transfer. *3rd International Conference on Mechanical, Automotive and Materials (ICMAME'2013) April 29-30, 2013 Singapore* **2013**.

34. Prasher, R.S.; Simmons, C.; Solbrekken, G. Thermal Contact Resistance of Phase Change and Grease Type Polymeric Materials. In Proceedings of the International Mechanical Engineering Congress and Exposition, Orlando, Florida; 2000; Vol. 11, pp. 461–466.

35. Yeh, C.L.; Wen, C.Y.; Chen, Y.F.; Yeh, S.H.; Wu, C.H. An Experimental Investigation of Thermal Contact Conductance Across Bolted Joints. *Experimental Thermal and Fluid Science* **2001**, *25*, 349–357, doi:10.1016/S0894-1777(01)00096-6.

36. Xu, R.; Xu, L. An Experimental Investigation of Thermal Contact Conductance of Stainless Steel at Low Temperatures. *Cryogenics* **2005**, *45*, 694–704, doi:10.1016/j.cryogenics.2005.09.002.

37. Shaikh, S.; Lafdi, K.; Silverman, E. The Effect of a CNT Interface on the Thermal Resistance of Contacting Surfaces. *Carbon* **2007**, *45*, 695–703, doi:10.1016/j.carbon.2006.12.007.

38. Saito, Y.; Suzuki, S.; Komuro, T. Evaluation of Thermal Interface Material With Electric Capacitance Measurement: A New Method Using Metal Meshes to Present Finer Surface Roughness Levels. In Proceedings of the IEEE CPMT Symposium Japan 2014; November 2014; pp. 11–14.

39. Chu, R.-S.; Zhao, Y.; Grigoropoulos, C.P. Effect of Copper Surface Roughness on Thermal Conductance of Copper/Carbon Nanotube Array Interface. In Proceedings of the 13th InterSociety Conference on Thermal and Thermomechanical Phenomena in Electronic Systems; May 2012; pp. 10–14.

40. Hong, Y.; Li, L.; Zeng, X.C.; Zhang, J. Tuning Thermal Contact Conductance at Graphene-Copper Interface via Surface Nanoengineering. *Nanoscale* **2015**, *7*, 6286–6294, doi:10.1039/c5nr00564g.

41. Karthick, K.; Joy, G.C.; Suresh, S.; Dhanuskodi, R. Impact of Thermal Interface Materials for Thermoelectric Generator Systems. *Journal of Electronic Materials* 2018, *47*, 5763–5772.

42. Hatakeyama, T.; Kibushi, R.; Ishizuka, M.; Tomimura, T. Fundamental Study of Surface Roughness Dependance of Thermal and Electrical Contact Resistance. In Proceedings of the 15th IEEE InterSociety Conference on

Thermal and Thermomechanical Phenomena in Electronic Systems (ITherm); 2016; pp. 1078–1082.

43. Hyodo, Y.; Hatakeyama, T.; Kibushi, R.; Ishizuka, M. Measurement of Thermal and Electrical Contact Resistance Between Conductive Materials. In Proceedings of the International Conference on Electronics Packaging and iMAPS All Asia Conference (ICEP-IAAC); 2018; pp. 132–135.

44. Shtein, M.; Nadiv, R.; Buzaglo, M.; Kahil, K.; Regev, O. Thermally Conductive Graphene-Polymer Composites: Size, Percolation, and Synergy Effects. *Chemistry of Materials* **2015**, *27*, 2100–2106, doi:10.1021/cm504550e.

45. Kim, H.S.; Bae, H.S.; Yu, J.; Kim, S.Y. Thermal Conductivity of Polymer Composites with the Geometrical Characteristics of Graphene Nanoplatelets. *Scientific Reports* **2016**, *6*, 26825, doi:10.1038/srep26825.

46. Shen, X.; Wang, Z.; Wu, Y.; Liu, X.; He, Y.-B.; Kim, J.-K. Multilayer Graphene Enables Higher Efficiency in Improving Thermal Conductivities of Graphene/Epoxy Composites. *Nano Letters* **2016**, *16*, 3585–3593, doi:10.1021/acs.nanolett.6b00722.

47. Devpura, A.; Phelan, P.E.; Prasher, R.S. Size Effects on the Thermal Conductivity of Pplymers Laden with Highly Conductive Filler Particles. *Microscale Thermophysical Engineering* **2001**, *5*, 177–189, doi:10.1080/108939501753222869.

48. Guoqing Zhang; Yanping Xia; Hui Wang; Yu Tao; Guoliang Tao; Shantung Tu; Haiping Wu A Percolation Model of Thermal Conductivity for Filled Polymer Composites. *Journal of Composite Materials* **2010**, *44*, 963–970, doi:10.1177/0021998309349690.

49. Debelak, B.; Lafdi, K. Use of Exfoliated Graphite Filler to Enhance Polymer Physical Properties. *Carbon* **2007**, *45*, 1727–1734, doi:10.1016/j.carbon.2007.05.010.

50. Ghosh, S.; Bao, W.; Nika, D.L.; Subrina, S.; Pokatilov, E.P.; Lau, C.N.; Balandin, A.A. Dimensional Crossover of Thermal Transport in Few-Layer Graphene. *Nature Materials* **2010**, *9*, 555–558, doi:10.1038/nmat2753.

51. Mahanta, N.K.; Loos, M.R.; Manas Zlocozower, I.; Abramson, A.R. Graphite–Graphene Hybrid Filler System for High Thermal Conductivity of Epoxy Composites. *Journal of Materials Research* **2015**, *30*, 959–966, doi:10.1557/jmr.2015.68.

52. Owais, M.; Zhao, J.; Imani, A.; Wang, G.; Zhang, H.; Zhang, Z. Synergetic Effect of Hybrid Fillers of Boron Nitride, Graphene Nanoplatelets, and Short Carbon Fibers for Enhanced Thermal Conductivity and Electrical Resistivity of Epoxy Nanocomposites. *Composites Part A: Applied Science and Manufacturing* **2019**, *117*, 11–22, doi:10.1016/j.compositesa.2018.11.006.

53. Senturk, A.E.; Oktem, A.S.; Konukman, A.E.S. Investigation of Interfacial Thermal Resistance of Hybrid Graphene/Hexagonal Boron Nitride. *International Journal of Mechanics and Materials in Design* **2019**, *15*, 727–737, doi:10.1007/s10999-018-09440-y.

54. Moradi, S.; Calventus, Y.; Román, F.; Hutchinson, J.M. Achieving High Thermal Conductivity in Epoxy Composites: Effect of Boron Nitride Particle Size and Matrix-Filler Interface. *Polymers* **2019**, *11*, 1156, doi:10.3390/polym11071156.

55. Zhou, W.-Y.; Qi, S.-H.; Zhao, H.-Z.; Liu, N.-L. Thermally Conductive Silicone Rubber Reinforced with Boron Nitride Particle. *Polymer Composites* **2007**, *28*, 23–28, doi:10.1002/pc.20296.

56. Pawelski, C.; Kang, E.; Bakis, G.; Altstädt, V. Effect of Filler Type and Particle Size Distribution on Thermal Properties of Bimodal and Hybrid – BN/Boehmite-Filled EP-Novolac Composites. In Proceedings of the AIP Conference Proceedings; 2019; p. 050007.

57. Tanimoto, M.; Yamagata, T.; Miyata, K.; Ando, S. Anisotropic Thermal Diffusivity of Hexagonal Boron Nitride-Filled Polyimide Films: Effects of Filler Particle Size, Aggregation, Orientation, and Polymer Chain Rigidity. *ACS Applied Materials & Interfaces* **2013**, *5*, 4374–4382, doi:10.1021/am400615z.

58. Ashraf, M.A.; Peng, W.; Zare, Y.; Rhee, K.Y. Effects of Size and Aggregation/Agglomeration of Nanoparticles on the Interfacial/Interphase Properties and Tensile Strength of Polymer Nanocomposites. *Nanoscale Research Letters* **2018**, *13*, 214, doi:10.1186/s11671-018-2624-0.

59. Jasmee, S.; Omar, G.; Othaman, S.S.C.; Masripan, N.A.; A. Hamid, H. Interface Thermal Resistance and Thermal Conductivity of Polymer Composites at Different Types, Shapes, and Sizes of Fillers: A Review. *Polymer Composites* **2021**, *42*, 2629–2652, doi:10.1002/pc.26029.

60. Sarvar, F.; Whalley, David.C.; Conway, Paul.P. Thermal Interface Materials - A Review of the State of the Art. *1st Electronic Systemintegration Technology Conference, Dresden, Germany* **2006**, 1292–1302.

61. Balandin, A.A. Phononics of Graphene and Related Materials. *ACS Nano* **2020**, *14*, 5170–5178, doi:10.1021/acsnano.0c02718.

62. Lewis, J.S.; Perrier, T.; Barani, Z.; Kargar, F.; Balandin, A.A. Thermal Interface Materials with Graphene Fillers: Review of the State of the Art and Outlook of Future Applications. *Nanotechnology* **2020**, doi:10.1088/1361-6528/abc0c6.

63. Renteria, J.; Legedza, S.; Salgado, R.; Balandin, M.P.; Ramirez, S.; Saadah, M.; Kargar, F.; Balandin, A.A. *Magnetically-Functionalized Self-Aligning Graphene Fillers for High-Efficiency Thermal Management Applications*; 2015;

64. Renteria, J.; Nika, D.; Balandin, A. Graphene Thermal Properties: Applications in Thermal Management and Energy Storage. *Applied Sciences* **2014**, *4*, 525–547, doi:10.3390/app4040525.

65. Malekpour, H.; Chang, K.-H.; Chen, J.-C.; Lu, C.-Y.; Nika, D.L.; Novoselov, K.S.; Balandin, A.A. Thermal Conductivity of Graphene Laminate. *Nano Letters* **2014**, *14*, 5155–5161, doi:10.1021/nl501996v.

66. Nika, D.L.; Yan, Z.; Balandin, A.A. Thermal Properties of Graphene and Few-Layer Graphene: Applications in Electronics. *IET Circuits, Devices & Systems* **2015**, *9*, 4–12, doi:10.1049/iet-cds.2014.0093.

67. Kargar, F.; Barani, Z.; Salgado, R.; Debnath, B.; Lewis, J.S.; Aytan, E.; Lake, R.K.; Balandin, A.A. Thermal Percolation Threshold and Thermal Properties of Composites with High Loading of Graphene and Boron Nitride Fillers. *ACS Applied Materials and Interfaces* **2018**, *10*, 37555–37565, doi:10.1021/acsami.8b16616.

68. Chung, D.D.L. Thermal Interface Materials. *Journal of Electronic Materials* 2020, *49*, 268–270.

69. Naghibi, S.; Kargar, F.; Wright, D.; Huang, C.Y.T.; Mohammadzadeh, A.; Barani, Z.; Salgado, R.; Balandin, A.A. Noncuring Graphene Thermal Interface Materials for Advanced Electronics. *Advanced Electronic Materials* **2020**, 1901303, doi:10.1002/aelm.201901303.

70. Saadah, M.; Gamalath, D.; Hernandez, E.; Balandin, A.A. Graphene-Enhanced Thermal Interface Materials for Heat Removal from Photovoltaic Solar Cells. In Proceedings of the Carbon Nanotubes, Graphene, and Emerging 2D Materials for Electronic and Photonic Devices IX; SPIE, September 26 2016; Vol. 9932, p. 99320H.

71. Saadah, M.; Hernandez, E.; Balandin, A.A. Thermal Management of Concentrated Multi-Junction Solar Cells with Graphene-Enhanced Thermal Interface Materials. *Applied Sciences (Switzerland)* **2017**, *7*, doi:10.3390/app7060589.

72. Mahadevan, B.K.; Naghibi, S.; Kargar, F.; Balandin, A.A. Non-Curing Thermal Interface Materials with Graphene Fillers for Thermal Management of Concentrated Photovoltaic Solar Cells. *C — Journal of Carbon Research* **2019**, *6*, 2, doi:10.3390/c6010002.

73. Novoselov, K.S.; Geim, A.K.; Morozov, S. v.; Jiang, D.; Zhang, Y.; Dubonos, S. v.; Grigorieva, I. v.; Firsov, A.A. Electric Field Effect in Atomically Thin Carbon Films. *Science* **2004**, *306*, 666–669, doi:10.1126/science.1102896.

74. Novoselov, K.S.; Geim, A.K.; Morozov, S. v.; Jiang, D.; Katsnelson, M.I.; Grigorieva, I. v.; Dubonos, S. v.; Firsov, A.A. Two-Dimensional Gas of Massless Dirac Fermions in Graphene. *Nature* **2005**, *438*, 197–200, doi:10.1038/nature04233.

75. Geim, A.K.; Novoselov, K.S. The Rise of Graphene. *Nature Materials* **2007**, *6*, 183–191, doi:10.1038/nmat1849.

76. Zhang, Y.; Tan, Y.-W.; Stormer, H.L.; Kim, P. Experimental Observation of the Quantum Hall Effect and Berry's Phase in Graphene. *Nature* **2005**, *438*, 201–204, doi:10.1038/nature04235.

77. Lee, C.; Wei, X.; Kysar, J.W.; Hone, J. Measurement of the Elastic Properties and Intrinsic Strength of Monolayer Graphene. *Science* **2008**, *321*, 385–388, doi:10.1126/science.1157996.

78. Nika, D.L.; Pokatilov, E.P.; Askerov, A.S.; Balandin, A.A. Phonon Thermal Conduction in Graphene: Role of Umklapp and Edge Roughness Scattering. *Physical Review B* **2009**, *79*, 155413, doi:10.1103/PhysRevB.79.155413.

79. Nika, D.L.; Ghosh, S.; Pokatilov, E.P.; Balandin, A.A. Lattice Thermal Conductivity of Graphene Flakes: Comparison with Bulk Graphite. *Applied Physics Letters* **2009**, *94*, 203103, doi:10.1063/1.3136860.

80. Ghosh, S.; Nika, D.L.; Pokatilov, E.P.; Balandin, A.A. Heat Conduction in Graphene: Experimental Study and Theoretical Interpretation. *New Journal of Physics* **2009**, *11*, 095012, doi:10.1088/1367-2630/11/9/095012.

81. Balandin, A.A.; Ghosh, S.; Nika, D.L.; Pokatilov, E.P. Thermal Conduction in Suspended Graphene Layers. *Fullerenes, Nanotubes and Carbon Nanostructures* **2010**, *18*, 474–486, doi:10.1080/1536383X.2010.487785.

82. Balandin, A.A. Thermal Properties of Graphene and Nanostructured Carbon Materials. *Nature Materials* **2011**, *10*, 569–581, doi:10.1038/nmat3064.

83. Ghosh, S.; Calizo, I.; Teweldebrhan, D.; Pokatilov, E.P.; Nika, D.L.; Balandin, A.A.; Bao, W.; Miao, F.; Lau, C.N. Extremely High Thermal Conductivity of Graphene: Prospects for Thermal Management Applications in Nanoelectronic Circuits. *Applied Physics Letters* **2008**, *92*, 151911, doi:10.1063/1.2907977.

84. Balandin, A.A.; Ghosh, S.; Bao, W.; Calizo, I.; Teweldebrhan, D.; Miao, F.; Lau, C.N. Superior Thermal Conductivity of Single-Layer Graphene. *Nano Letters* **2008**, *8*, 902–907, doi:10.1021/nl0731872.

85. Neugebauer, P.; Orlita, M.; Faugeras, C.; Barra, A.-L.; Potemski, M. How Perfect Can Graphene Be? *Physical Review Letters* **2009**, *103*, 136403, doi:10.1103/PhysRevLett.103.136403.

86. Banszerus, L.; Schmitz, M.; Engels, S.; Dauber, J.; Oellers, M.; Haupt, F.; Watanabe, K.; Taniguchi, T.; Beschoten, B.; Stampfer, C. Ultrahigh-Mobility Graphene Devices from Chemical Vapor Deposition on Reusable Copper. *Science Advances* **2015**, *1*, e1500222, doi:10.1126/sciadv.1500222.

87. Jaćimovski, S.K.; Bukurov, M.; Šetrajčić, J.P.; Raković, D.I. Phonon Thermal Conductivity of Graphene. *Superlattices and Microstructures* **2015**, *88*, 330–337, doi:10.1016/j.spmi.2015.09.027.

88. Goyal, V.; Balandin, A.A. Thermal Properties of the Hybrid Graphene-Metal Nano-Micro-Composites: Applications in Thermal Interface Materials. *Applied Physics Letters* **2012**, *100*, 073113, doi:10.1063/1.3687173.

89. Lewis, J.S.; Perrier, T.; Mohammadzadeh, A.; Kargar, F.; Balandin, A.A. Power Cycling and Reliability Testing of Epoxy-Based Graphene Thermal Interface Materials. *C — Journal of Carbon Research* **2020**, *6*, 26, doi:10.3390/c6020026.

90. Fu, Y.; Hansson, J.; Liu, Y.; Chen, S.; Zehri, A.; Samani, M.K.; Wang, N.; Ni, Y.; Zhang, Y.; Zhang, Z.-B.; et al. Graphene Related Materials for Thermal Management. *2D Materials* **2020**, *7*, 012001, doi:10.1088/2053-1583/ab48d9.

91. Lewis, J.S. Reduction of Device Operating Temperatures with Graphene-Filled Thermal Interface Materials. *C — Journal of Carbon Research* **2021**, *7*, 53, doi:10.3390/c7030053.

92. Xie, X.; Yang, K.; Li, D.; Tsai, T.-H.; Shin, J.; Braun, P. v.; Cahill, D.G. High and Low Thermal Conductivity of Amorphous Macromolecules. *Physical Review B* **2017**, *95*, 035406, doi:10.1103/PhysRevB.95.035406.

93. Kargar, F.; Barani, Z.; Balinskiy, M.; Magana, A.S.; Lewis, J.S.; Balandin, A.A. Dual-Functional Graphene Composites for Electromagnetic Shielding and Thermal Management. *Advanced Electronic Materials* **2019**, *5*, doi:10.1002/aelm.201800558.

94. Lewis, J.S.; Barani, Z.; Magana, A.S.; Kargar, F.; Balandin, A.A. Thermal and Electrical Conductivity Control in Hybrid Composites with Graphene and Boron Nitride Fillers. *Materials Research Express* **2019**, *6*, doi:10.1088/2053-1591/ab2215.

95. Barani, Z.; Mohammadzadeh, A.; Geremew, A.; Huang, C.Y.; Coleman, D.; Mangolini, L.; Kargar, F.; Balandin, A.A. Thermal Properties of the Binary-Filler Hybrid Composites with Graphene and Copper Nanoparticles. *Advanced Functional Materials* **2019**, doi:10.1002/adfm.201904008.

96. Yan, Z.; Liu, G.; Khan, J.M.; Balandin, A.A. Graphene Quilts for Thermal Management of High-Power GaN Transistors. *Nature Communications* **2012**, *3*, 827, doi:10.1038/ncomms1828.

97. Goli, P.; Ning, H.; Li, X.; Lu, C.Y.; Novoselov, K.S.; Balandin, A.A. Thermal Properties of Graphene-Copper-Graphene Heterogeneous Films. *Nano Letters* **2014**, *14*, 1497–1503, doi:10.1021/nl404719n.

98. Goli, P.; Legedza, S.; Dhar, A.; Salgado, R.; Renteria, J.; Balandin, A.A. Graphene-Enhanced Hybrid Phase Change Materials for Thermal Management of Li-Ion Batteries. *Journal of Power Sources* **2014**, *248*, 37–43, doi:10.1016/j.jpowsour.2013.08.135.

99. Barani, Z.; Kargar, F.; Mohammadzadeh, A.; Naghibi, S.; Lo, C.; Rivera, B.; Balandin, A.A. Multifunctional Graphene Composites for Electromagnetic Shielding and Thermal Management at Elevated Temperatures. *Advanced*

Electronic Materials **2020**, *6*, 2000520-undefined, doi:10.1002/aelm.202000520.

100. Barani, Z.; Kargar, F.; Godziszewski, K.; Rehman, A.; Yashchyshyn, Y.; Rumyantsev, S.; Cywiński, G.; Knap, W.; Balandin, A.A. Graphene Epoxy-Based Composites as Efficient Electromagnetic Absorbers in the Extremely High-Frequency Band. *ACS Applied Materials and Interfaces* **2020**, *12*, 28635–28644, doi:10.1021/acsami.0c06729.

101. Wang, Z.-G.; Lv, J.-C.; Zheng, Z.-L.; Du, J.-G.; Dai, K.; Lei, J.; Xu, L.; Xu, J.-Z.; Li, Z.-M. Highly Thermally Conductive Graphene-Based Thermal Interface Materials with a Bilayer Structure for Central Processing Unit Cooling. *ACS Applied Materials & Interfaces* **2021**, doi:10.1021/acsami.1c01223.

102. Yu, W.; Xie, H.; Chen, L.; Zhu, Z.; Zhao, J.; Zhang, Z. Graphene Based Silicone Thermal Greases. *Physics Letters A* **2014**, *378*, 207–211, doi:10.1016/j.physleta.2013.10.017.

103. Abbott, J.P.R.; Zhu, H. 3D Optical Surface Profiler for Quantifying Leaf Surface Roughness. *Surface Topography: Metrology and Properties* **2019**, *7*, doi:10.1088/2051-672X/ab4cc6.

104. Hadi, S.; Aqiftiar Falah, F.; Kurniawan, A.; Suyitno The Design of High-Temperature Thermal Conductivity Measurements Apparatus for Thin Sample Size. *MATEC Web of Conferences* **2017**, *101*, 03007, doi:10.1051/matecconf/201710103007.

105. Buliński, Z.; Pawlak, S.; Krysiński, T.; Adamczyk, W.; Białecki, R. Application of the ASTM D5470 Standard Test Method for Thermal Conductivity Measurements of High Thermal Conductive Materials. *Journal of Achievements in Materials and Manufacturing Engineering* **2019**, *95*, 57–63, doi:10.5604/01.3001.0013.7915.

106. Kim, Y.; Lee, J.; Yeom, M.S.; Shin, J.W.; Kim, H.; Cui, Y.; Kysar, J.W.; Hone, J.; Jung, Y.; Jeon, S.; et al. Strengthening Effect of Single-Atomic-Layer Graphene in Metal–Graphene Nanolayered Composites. *Nature Communications* **2013**, *4*, 2114, doi:10.1038/ncomms3114.

107. Li, X.; Zhao, Y.; Wu, W.; Chen, J.; Chu, G.; Zou, H. Synthesis and Characterizations of Graphene–Copper Nanocomposites and Their Antifriction Application. *Journal of Industrial and Engineering Chemistry* **2014**, *20*, 2043–2049, doi:10.1016/j.jiec.2013.09.029.

108. *XGnP® Graphene Nanoplatelets – Grade H , Product Specification Sheet*; xGnP® Graphene Nanoplatelets – Grade H, XG-Sciences, 2019;

109. Yu, A.; Ramesh, P.; Itkis, M.E.; Bekyarova, E.; Haddon, R.C. Graphite Nanoplatelet-Epoxy Composite Thermal Interface Materials. *Journal of Physical Chemistry C* **2007**, *111*, 7565–7569, doi:10.1021/jp071761s.

110. Burzo, M.G.; Raad, P.E.; Komarov, P.L.; Wicaksono, C.; Choi, T.Y. Measurement of Thermal Conductivity of Nanofluids and Thermal Interface Materials Using the Laser-Based Transient Thermoreflectance Method. In Proceedings of the 29th IEEE Semiconductor Thermal Measurement and Management Symposium; IEEE, March 2013; pp. 194–199.

111. Raza, M.A.; Westwood, A.; Stirling, C. Comparison of Carbon Nanofiller-Based Polymer Composite Adhesives and Pastes for Thermal Interface Applications. *Materials & Design* **2015**, *85*, 67–75, doi:10.1016/j.matdes.2015.07.008.

112. Prasher, R.S.; Shipley, J.; Prstic, S.; Koning, P.; Wang, J. Thermal Resistance of Particle Laden Polymeric Thermal Interface Materials. *Journal of Heat Transfer* **2003**, *125*, 1170–1177, doi:10.1115/1.1621893.

113. Evans, W.; Prasher, R.; Fish, J.; Meakin, P.; Phelan, P.; Keblinski, P. Effect of Aggregation and Interfacial Thermal Resistance on Thermal Conductivity of Nanocomposites and Colloidal Nanofluids. *International Journal of Heat and Mass Transfer* **2008**, *51*, 1431–1438, doi:10.1016/j.ijheatmasstransfer.2007.10.017.

114. Zhang, L.; Ruesch, M.; Zhang, X.; Bai, Z.; Liu, L. Tuning Thermal Conductivity of Crystalline Polymer Nanofibers by Interchain Hydrogen Bonding. *RSC Advances* **2015**, *5*, 87981–87986, doi:10.1039/C5RA18519J.

115. Mu, L.; Ji, T.; Chen, L.; Mehra, N.; Shi, Y.; Zhu, J. Paving the Thermal Highway with Self-Organized Nanocrystals in Transparent Polymer Composites. *ACS Applied Materials & Interfaces* **2016**, *8*, 29080–29087, doi:10.1021/acsami.6b10451.

116. Prasher, R.S.; Shipley, J.; Prstic, S.; Koning, P.; Wang, J.-L. Thermal Resistance of Particle Laden Polymeric Thermal Interface Materials. In Proceedings of the Electronic and Photonic Packaging, Electrical Systems and Photonic Design, and Nanotechnology; ASMEDC, January 1 2003; pp. 431–439.

117. Prasher, R.S.; Matayabas, J.C. Thermal Contact Resistance of Cured Gel Polymeric Thermal Interface Material. *Thermomechanical Phenomena in Electronic Systems -Proceedings of the Intersociety Conference* **2004**, *1*, 28–35, doi:10.1109/itherm.2004.1319150.

118. Narumanchi, S.; Mihalic, M.; Kelly, K.; Eesley, G. Thermal Interface Materials for Power Electronics Applications. In Proceedings of the 2008 11th IEEE Intersociety Conference on Thermal and Thermomechanical Phenomena in Electronic Systems, I-THERM; 2008; pp. 395–404.

119. Maguire, L.; Behnia, M.; Morrison, G. Systematic Evaluation of Thermal Interface Materials-a Case Study in High Power Amplifier Design. *Microelectronics Reliability* **2005**, *45*, 711–725, doi:10.1016/j.microrel.2004.10.030.

120. Skuriat, R.; Li, J.F.; Agyakwa, P.A.; Mattey, N.; Evans, P.; Johnson, C.M. Degradation of Thermal Interface Materials for High-Temperature Power Electronics Applications. *Microelectronics Reliability* **2013**, *53*, 1933–1942, doi:10.1016/j.microrel.2013.05.011.

121. Broughton, J.; Smet, V.; Tummala, R.R.; Joshi, Y.K. Review of Thermal Packaging Technologies for Automotive Power Electronics for Traction Purposes. *Journal of Electronic Packaging, Transactions of the ASME* **2018**, *140*, 1–11, doi:10.1115/1.4040828.

122. Hernandez, Y.; Nicolosi, V.; Lotya, M.; Blighe, F.M.; Sun, Z.; De, S.; McGovern, I.T.; Holland, B.; Byrne, M.; Gun'Ko, Y.K.; et al. High-Yield Production of Graphene by Liquid-Phase Exfoliation of Graphite. *Nature Nanotechnology* **2008**, *3*, 563–568, doi:10.1038/nnano.2008.215.

123. Lotya, M.; Hernandez, Y.; King, P.J.; Smith, R.J.; Nicolosi, V.; Karlsson, L.S.; Blighe, F.M.; De, S.; Wang, Z.; McGovern, I.T.; et al. Liquid Phase Production of Graphene by Exfoliation of Graphite in Surfactant/Water Solutions. *Journal of the American Chemical Society* **2009**, *131*, 3611–3620, doi:10.1021/ja807449u.

124. Nicolosi, V.; Chhowalla, M.; Kanatzidis, M.G.; Strano, M.S.; Coleman, J.N. Liquid Exfoliation of Layered Materials. *Science* **2013**, *340*, 1226419–1226419, doi:10.1126/science.1226419.

125. Tao, H.; Zhang, Y.; Gao, Y.; Sun, Z.; Yan, C.; Texter, J. Scalable Exfoliation and Dispersion of Two-Dimensional Materials – an Update. *Physical Chemistry Chemical Physics* **2017**, *19*, 921–960, doi:10.1039/C6CP06813H.

126. Bonaccorso, F.; Bartolotta, A.; Coleman, J.N.; Backes, C. 2D-Crystal-Based Functional Inks. *Advanced Materials* **2016**, *28*, 6136–6166, doi:10.1002/adma.201506410.

127. Backes, C.; Szydłowska, B.M.; Harvey, A.; Yuan, S.; Vega-Mayoral, V.; Davies, B.R.; Zhao, P.; Hanlon, D.; Santos, E.J.G.; Katsnelson, M.I.; et al. Production of Highly Monolayer Enriched Dispersions of Liquid-Exfoliated Nanosheets by Liquid Cascade Centrifugation. *ACS Nano* **2016**, *10*, 1589–1601, doi:10.1021/acsnano.5b07228.

128. Backes, C.; Paton, K.R.; Hanlon, D.; Yuan, S.; Katsnelson, M.I.; Houston, J.; Smith, R.J.; McCloskey, D.; Donegan, J.F.; Coleman, J.N. Spectroscopic Metrics Allow in Situ Measurement of Mean Size and Thickness of Liquid-Exfoliated Few-Layer Graphene Nanosheets. *Nanoscale* **2016**, *8*, 4311–4323, doi:10.1039/C5NR08047A.

129. Sudhindra, S.; Rashvand, F.; Wright, D.; Barani, Z.; Drozdov, A.D.; Baraghani, S.; Backes, C.; Kargar, F.; Balandin, A.A. Thermal Transport in Graphene Composites: The Effect of Lateral Dimensions of Graphene Fillers. *Archive* **2021**, 1–38.

130. Backes, C.; Campi, D.; Szydlowska, B.M.; Synnatschke, K.; Ojala, E.; Rashvand, F.; Harvey, A.; Griffin, A.; Sofer, Z.; Marzari, N.; et al. Equipartition of Energy Defines the Size–Thickness Relationship in Liquid-Exfoliated Nanosheets. *ACS Nano* **2019**, *13*, 7050–7061, doi:10.1021/acsnano.9b02234.

131. Lewis, J.S.; Perrier, T.; Barani, Z.; Kargar, F.; Balandin, A.A. Thermal Interface Materials with Graphene Fillers: Review of the State of the Art and Outlook of Future Applications. *Nanotechnology* **2021**, *32*, 142003, doi:10.1088/1361-6528/abc0c6.

132. Balandin, A.A.; Ghosh, S.; Nika, D.L.; Pokatilov, E.P. Thermal Conduction in Suspended Graphene Layers. *Fullerenes, Nanotubes and Carbon Nanostructures* **2010**, *18*, 474–486, doi:10.1080/1536383X.2010.487785.

133. Nika, D.L.; Askerov, A.S.; Balandin, A.A. Anomalous Size Dependence of the Thermal Conductivity of Graphene Ribbons. *Nano Letters* **2012**, *12*, 3238–3244, doi:10.1021/nl301230g.

134. Nika, D.L.; Balandin, A.A. Two-Dimensional Phonon Transport in Graphene. *Journal of Physics: Condensed Matter* **2012**, *24*, 233203, doi:10.1088/0953-8984/24/23/233203.

135. Balandin, A.A.; Nika, D.L. Phononics in Low-Dimensional Materials. *Materials Today* **2012**, *15*, 266–275, doi:10.1016/S1369-7021(12)70117-7.

136. Ferrari, A.C.; Meyer, J.C.; Scardaci, V.; Casiraghi, C.; Lazzeri, M.; Mauri, F.; Piscanec, S.; Jiang, D.; Novoselov, K.S.; Roth, S.; et al. Raman Spectrum of Graphene and Graphene Layers. *Physical Review Letters* **2006**, *97*, 187401, doi:10.1103/PhysRevLett.97.187401.

137. Calizo, I.; Balandin, A.A.; Bao, W.; Miao, F.; Lau, C.N. Temperature Dependence of the Raman Spectra of Graphene and Graphene Multilayers. *Nano Letters* **2007**, *7*, 2645–2649, doi:10.1021/nl071033g.

138. Calizo, I.; Teweldebrhan, D.; Bao, W.; Miao, F.; Lau, C.N.; Balandin, A.A. Spectroscopic Raman Nanometrology of Graphene and Graphene Multilayers on Arbitrary Substrates. *Journal of Physics: Conference Series* **2008**, *109*, 012008, doi:10.1088/1742-6596/109/1/012008.

139. Gupta, A.; Chen, G.; Joshi, P.; Tadigadapa, S.; Eklund Raman Scattering from High-Frequency Phonons in Supported n -Graphene Layer Films. *Nano Letters* **2006**, *6*, 2667–2673, doi:10.1021/nl061420a.

140. Graf, D.; Molitor, F.; Ensslin, K.; Stampfer, C.; Jungen, A.; Hierold, C.; Wirtz, L. Spatially Resolved Raman Spectroscopy of Single- and Few-Layer Graphene. *Nano Letters* **2007**, *7*, 238–242, doi:10.1021/nl061702a.

141. Malard, L.M.; Pimenta, M.A.; Dresselhaus, G.; Dresselhaus, M.S. Raman Spectroscopy in Graphene. *Physics Reports* **2009**, *473*, 51–87, doi:10.1016/j.physrep.2009.02.003.

142. Khan, U.; O'Neill, A.; Porwal, H.; May, P.; Nawaz, K.; Coleman, J.N. Size Selection of Dispersed, Exfoliated Graphene Flakes by Controlled Centrifugation. *Carbon* **2012**, *50*, 470–475, doi:10.1016/j.carbon.2011.09.001.

143. Parvizi, F.; Teweldebrhan, D.; Ghosh, S.; Calizo, I.; Balandin, A.A.; Zhu, H.; Abbaschian, R. Properties of Graphene Produced by the High Pressure–High Temperature Growth Process. *Micro & Nano Letters* **2008**, *3*, 29, doi:10.1049/mnl:20070074.

144. Teweldebrhan, D.; Balandin, A.A. Modification of Graphene Properties Due to Electron-Beam Irradiation. *Applied Physics Letters* **2009**, *94*, 013101, doi:10.1063/1.3062851.

145. Silva, D.L.; Campos, J.L.E.; Fernandes, T.F.D.; Rocha, J.N.; Machado, L.R.P.; Soares, E.M.; Miquita, D.R.; Miranda, H.; Rabelo, C.; Vilela Neto, O.P.; et al. Raman Spectroscopy Analysis of Number of Layers in Mass-Produced Graphene Flakes. *Carbon* **2020**, *161*, 181–189, doi:10.1016/j.carbon.2020.01.050.

146. Hurley, S.; Cann, P.M.; Spikes, H.A. Lubrication and Reflow Properties of Thermally Aged Greases. *Tribology Transactions* **2000**, *43*, 221–228, doi:10.1080/10402000008982332.

147. Mortezaei, M.; Farzi, G.; Kalaee, M.R.; Zabihpoor, M. Evaluation of Interfacial Layer Properties in the Polystyrene/Silica Nanocomposite. *Journal of Applied Polymer Science* **2011**, *119*, 2039–2047, doi:10.1002/app.32902.

148. Mortezaei, M.; Famili, M.H.N.; Kokabi, M. Influence of the Particle Size on the Viscoelastic Glass Transition of Silica-Filled Polystyrene. *Journal of Applied Polymer Science* **2010**, *115*, 969–975, doi:10.1002/app.31048.

149. Wang, J. Shear Modulus Measurement for Thermal Interface Materials in Flip Chip Packages. *IEEE Transactions on Components and Packaging Technologies* **2006**, *29*, 610–617, doi:10.1109/TCAPT.2006.880505.

150. Iisaka, K.; Shibayama, K. Effect of Filler Particle Size on Dynamic Mechanical Properties of Poly(Methyl Methacrylate). *Journal of Applied Polymer Science* **1978**, *22*, 1321–1330, doi:10.1002/app.1978.070220513.

151. Wu, X.; Lin, T.F.; Tang, Z.H.; Guo, B.C.; Huang, G.S. Natural Rubber/Graphene Oxide Composites: Effect of Sheet Size on Mechanical Properties and Strain-Induced Crystallization Behavior. *Express Polymer Letters* **2015**, *9*, 672–685, doi:10.3144/expresspolymlett.2015.63.

152. Robertson, C.G.; Lin, C.J.; Rackaitis, M.; Roland, C.M. Influence of Particle Size and Polymer−Filler Coupling on Viscoelastic Glass Transition of Particle-Reinforced Polymers. *Macromolecules* **2008**, *41*, 2727–2731, doi:10.1021/ma7022364.

153. Hristov, V.; Vlachopoulos, J. Effects of Polymer Molecular Weight and Filler Particle Size on Flow Behavior of Wood Polymer Composites. *Polymer Composites* **2008**, *29*, 831–839, doi:10.1002/pc.20455.

154. Osman, M.A.; Atallah, A. Effect of the Particle Size on the Viscoelastic Properties of Filled Polyethylene. *Polymer* **2006**, *47*, 2357–2368, doi:10.1016/j.polymer.2006.01.085.

155. McGrath, L.M.; Parnas, R.S.; King, S.H.; Schroeder, J.L.; Fischer, D.A.; Lenhart, J.L. Investigation of the Thermal, Mechanical, and Fracture Properties of Alumina–Epoxy Composites. *Polymer* **2008**, *49*, 999–1014, doi:10.1016/j.polymer.2007.12.014.

156. Kourki, H.; Famili, M.H.N.; Mortezaei, M.; Malekipirbazari, M.; Disfani, M.N. Highly Nanofilled Polystyrene Composite. *Journal of Elastomers & Plastics* **2016**, *48*, 404–425, doi:10.1177/0095244315580455.

157. Shenoy, A. v. *Rheology of Filled Polymer Systems*; Springer Netherlands: Dordrecht, 1999; ISBN 978-90-481-4029-9.

158. Prasher, R.S.; Koning, P.; Shipley, J.; Devpura, A. Dependence of Thermal Conductivity and Mechanical Rigidity of Particle-Laden Polymeric Thermal Interface Material on Particle Volume Fraction. *Journal of Electronic Packaging* **2003**, *125*, 386–391, doi:10.1115/1.1602703.

159. Bae, M.-H.; Li, Z.; Aksamija, Z.; Martin, P.N.; Xiong, F.; Ong, Z.-Y.; Knezevic, I.; Pop, E. Ballistic to Diffusive Crossover of Heat Flow in Graphene Ribbons. *Nature Communications* **2013**, *4*, 1734, doi:10.1038/ncomms2755.

160. Kanari, K. Thermal Conductivity of Composite Materials (In Japanese). *Kobunshi* **1977**, *26*, 557–561, doi:10.1295/kobunshi.26.557.

161. Bruggeman, D.A.G. Berechnung Verschiedener Physikalischer Konstanten von Heterogenen Substanzen. *Annals of Physics* **1935**, *24*, 636–679.

162. Drozdov, A.D.; deClaville Christiansen, J. Modeling Thermal Conductivity of Highly Filled Polymer Composites. *Polymer Engineering & Science* **2019**, *59*, 2174–2179, doi:10.1002/pen.25220.

163. Raza, M.A.; Westwood, A.V.K.; Stirling, C. Graphite Nanoplatelet/Silicone Composites for Thermal Interface Applications. *International Symposium on Advanced Packaging Materials: Microtech (APM), Cambridge* **2010**, 34–48.

164. Raza, M.A.; Westwood, A.; Brown, A.; Hondow, N.; Stirling, C. Characterisation of Graphite Nanoplatelets and the Physical Properties of Graphite Nanoplatelet/Silicone Composites for Thermal Interface Applications. *Carbon* **2011**, *49*, 4269–4279, doi:10.1016/j.carbon.2011.06.002.

165. Raza, M.A.; Westwood, A.V.K.; Brown, A.P.; Stirling, C. Texture, Transport and Mechanical Properties of Graphite Nanoplatelet/Silicone Composites

Produced by Three Roll Mill. *Composites Science and Technology* **2012**, *72*, 467–475, doi:10.1016/j.compscitech.2011.12.010.